Assessing Climate Change-Induced Flood Risk in the Conasauga River Watershed: An Application of Ensemble Hydrodynamic Inundation Modeling

Tigstu T. Dullo[1], George K. Darkwah[1], Sudershan Gangrade[2,3], Mario Morales-Hernández[3,4], Md Bulbul Sharif[5], Alfred J. Kalyanapu[1,*], Shih-Chieh Kao[2,3], Sheikh Ghafoor[5], and Moetasim Ashfaq[3,4]

[1] Department of Civil and Environmental Engineering, Tennessee Technological University, Cookeville, TN 38505, USA
[2] Environmental Sciences Division, Oak Ridge National Laboratory, Oak Ridge, TN 37831, USA
[3] Climate Change Science Institute, Oak Ridge National Laboratory, Oak Ridge, TN 37831, USA
[4] Computational Sciences and Engineering Division, Oak Ridge National Laboratory, Oak Ridge, TN 37831, USA
[5] Department of Computer Science, Tennessee Technological University, Cookeville, TN 38505, USA

*Corresponding Author
Alfred J. Kalyanapu, PhD
1020 Stadium Drive, P O Box 5015
Cookeville, TN 38505
Telephone: 931-372-3561
Email Address: akalyanapu@tntech.edu

Abstract

This study evaluates the impact of potential future climate change on flood regimes, floodplain protection, and electricity infrastructures across the Conasauga River Watershed in the southeastern United States through ensemble hydrodynamic inundation modeling. The ensemble streamflow scenarios were simulated by the Distributed Hydrology Soil Vegetation Model (DHSVM) driven by (1) 1981–2012 Daymet meteorological observations, and (2) eleven sets of downscaled global climate models (GCMs) during the 1966–2005 historical and 2011–2050 future periods. Surface inundation was simulated using a GPU-accelerated Two-dimensional Runoff Inundation Toolkit for Operational Needs (TRITON) hydrodynamic model. Nine out of the eleven GCMs exhibit an increase in the mean ensemble flood inundation areas. Moreover, at the 1% annual exceedance probability level, the flood inundation frequency curves indicate a ~16 km^2 increase in floodplain area. The assessment also shows that even after flood-proofing, four of the substations could still be affected in the projected future period. The increase in floodplain area and substation vulnerability highlights the need to account for climate change in floodplain management. Overall, this study provides a proof-of-concept demonstration of how the computationally intensive hydrodynamic inundation modeling can be used to enhance flood frequency maps and vulnerability assessment under the changing climatic conditions.

Keywords: Flood simulation; Climate change; Critical electricity infrastructure; Floodplain protection standards.

1. Introduction

Floods are costly disasters that affect more people than any other natural hazard around the world (UNISDR, 2015). Major factors that can exacerbate flood damage include population growth, urbanization, and climate change (Birhanu et al., 2016; Winsemius et al., 2016; Alfieri et al., 2017; Alfieri et al., 2018; Kefi et al., 2018). Recent observations exhibit an increase in the frequency and the intensity of extreme precipitation events (Pachauri and Meyer, 2014), which have strengthened the magnitude and frequency of flooding (Milly et al., 2002; Langerwisch et al., 2013; Alfieri et al., 2015a; Alfieri et al., 2018; Mora et al., 2018). As a result, the damage and cost of flooding have substantially increased across the United States (US) (Pielke Jr. and Downton, 2000; Pielke Jr. et al., 2002; Ntelekos et al., 2010; Wing et al., 2018) and the rest of the world (Hirabayashi et al., 2013; Arnell and Gosling, 2014; Alfieri et al., 2015b; Alfieri et al., 2017; Kefi et al., 2018).

Since 1968, the National Flood Insurance Program (NFIP), administered by the Federal Emergency Management Agency (FEMA), has implemented floodplain regulation standards in the US to mitigate the escalating flood losses (FEMA, 2002). For communities participating in the NFIP, flood insurance is required for structures located within the 1% annual exceedance probability (AEP) flood zone (i.e., areas with probability of flooding $\geq$ 1% in any given year; FEMA, 2002). However, existing floodplain protection standards have proven to be inadequate (Galloway et al., 2006; Ntelekos et al., 2010; Tan, 2013; Blessing et al., 2017; HCFCD, 2018), and climate change can likely exacerbate these issues (Olsen, 2006; Ntelekos et al., 2010; Kollat et al., 2012; AECOM, 2013; Wobus et al., 2017; Nyaupane et al., 2018; Pralle, 2019). For

instance, the streamflow AEP thresholds and synthetic hydrographs used to simulate the flood zones were derived purely based on historic observations that may underestimate the intensified hydrologic extremes in the projected future climatic conditions. Although the possible change of future streamflow AEP thresholds may be evaluated by an ensemble of hydrologic model outputs driven by multiple downscaled and bias-corrected climate models (e.g., Wobus et al., 2017), the extension from maximum streamflow to maximum flood zone is not trivial, and cannot be explicitly addressed through the conventional deterministic inundation modeling approach.

The increases in the magnitude and frequency of flooding, in addition to the inadequacy of floodplain measures and the high costs of hardening (Wilbanks et al., 2008; Farber-DeAnda et al., 2010; Gilstrap et al., 2015), have put electricity infrastructures at risk (Zamuda et al., 2015; Zamuda and Lippert, 2016; Cronin et al., 2018; Forzieri et al., 2018; Mikellidou et al., 2018; Allen-Dumas et al., 2019). In particular, electricity infrastructures which lie in areas vulnerable to flooding can experience floodwater damages that may lead to changes in their energy production and consumption (Chandramowli and Felder, 2014; Ciscar and Dowling, 2014; Bollinger and Dijkema, 2016; Gangrade et al., 2019). For instance, flooding can rust metals, destroy insulation, and damage interruption capacity (Farber-DeAnda et al., 2010; Vale, 2014; NERC, 2018; Bragatto et al., 2019). It is estimated that nearly 300 energy facilities are located on low-lying lands vulnerable to sea-level rise and flooding in the lower 48 US states, (Strauss and Ziemlinski, 2012).

Several studies have assessed the vulnerability of electricity infrastructures to flooding (Reed et al., 2009; Winkler et al., 2010; Bollinger and Dijkema, 2016; Fu et al.,

2017; Pant et al., 2017; Bragatto et al., 2019; Gangrade et al., 2019). For highly sensitive water infrastructures such as dams (McCuen, 2005), Gangrade et al. (2019) showed that the surface inundation associated with probable maximum flood (PMF) is generally projected to increase in future climate conditions. However, given the extremely large magnitude of PMF (AEP < 10^{-4} %), the findings cannot be directly associated with more frequent and moderate flood events (i.e., AEP around 1–0.2%) that are the main focus of many engineering applications. Although some of these studies focused on evaluating the resilience of electricity infrastructures against flood hazard and/or climate change, only a few of them evaluated site-specific inundation risk and quantified impacts of climate change-induced flooding on electricity infrastructures under different future climate scenarios. Again, one main challenge is associated with the high computational costs to effectively transform ensemble streamflow projections into ensemble surface inundation projections through hydrodynamic models. With the enhanced inundation models and high-performance computing (HPC) capabilities (Morales-Hernández et al., 2020), this challenge can be gradually overcome for more spatially explicit flood vulnerability assessment.

The objective of this study is to demonstrate the applicability of a computationally intensive ensemble inundation modeling approach to better understand how climate change may affect flood regimes, floodplain regulation standards, and the vulnerability of existing infrastructures. Extending from the framework developed by Gangrade et al. (2019) for PMF-scale events (AEP < 10^{-4} %) based on one selected climate model (CCSM4), we focus on more frequent extreme streamflow events (i.e., AEP around 1–0.2%) which requires different modeling strategies based on multiple downscaled climate

models. The unique aspects of this study are the application of an integrated climate-hydrologic-hydraulic modeling framework for:

(1) Evaluating the changes in flood regime using high-resolution ensemble flood inundation maps. The ensemble-based approach is able to incorporate the large hydrologic interannual variability and model uncertainty that cannot be captured through the conventional deterministic flood map.

(2) Enabling direct frequency analysis of ensemble flood inundation maps that correspond to historic and projected future climate conditions. This approach provides an alternative floodplain delineation technique to the conventional approach, in which a single deterministic design flood value is used to develop a flood map with a given exceedance probability.

(3) Evaluating the vulnerability of electricity infrastructures to climate change-induced flooding and assessing the adequacy of existing flood protection measures using ensemble flood inundation. This information will help floodplain managers to identify the most vulnerable infrastructures and recommend suitable adaptation measures.

The following technique was adopted in this study. First, we generated streamflow projection by utilizing an ensemble of simulated streamflow hydrographs driven by both historical observations and downscaled climate projections (Gangrade et al., 2020) as inputs for hydrodynamic inundation modeling as presented in section 2.2. Then, we set up and calibrated a 2D hydrodynamic inundation model, Two-dimensional Runoff Inundation Toolkit for Operational Needs (TRITON; Morales-Hernández et al., 2021), in our study area which is presented in section 2.3. For inundation modeling, sensitivity

analyses were conducted on three selected parameters to quantify and compare their respective influences on modeled flood depths and extents. The performance of TRITON was then evaluated by comparing a simulated 1% AEP flood map with the reference 1% AEP flood map from the Federal Emergency Management Agency (FEMA). Finally, as presented in sections 2.4 and 2.5, ensemble inundation modeling was performed to develop flood inundation frequency curves and maps, and to assess the vulnerability of electricity infrastructures under a changing climate, respectively.

The article is organized as follows: the data and methods are discussed in Section 2; Section 3 presents the result and discussion; and the summary is presented in Section 4.

2. Data and Methods

2.1. Study Area

Our study area is the Conasauga River Watershed (CRW) located in southeastern Tennessee and northwestern Georgia (Figure 1). The CRW is an eight-digit Hydrologic Unit Code (HUC08) subbasin (03150101) with a total drainage area of ~1880 km^2. The northeastern portions of the watershed are rugged, mountainous areas largely covered with forests (Ivey and Evans, 2000; Elliott and Vose, 2005). The CRW, which is one headwater basin of the Alabama-Coosa-Tallapoosa (ACT) River Basin, rises high on the Blue Ridge Mountains of Georgia and Tennessee and flows for 145 km before joining the Coosawattee River to form the Oostanaula River (Ivey and Evans, 2000; USACE, 2013). The CRW climate is characterized by warm, humid summers, and mild winters with mean annual temperature of 15 to 20 ℃ and average annual precipitation of 1300 to 1400 mm (FIS, 2007; FIS, 2010; Baechler et al., 2015). The watershed encompasses four

counties: Bradley, Polk, Fannin, Murray, and Whitfield. It also includes the cities of Dalton and Chatsworth, Georgia. There is no major reservoir located in the CRW.

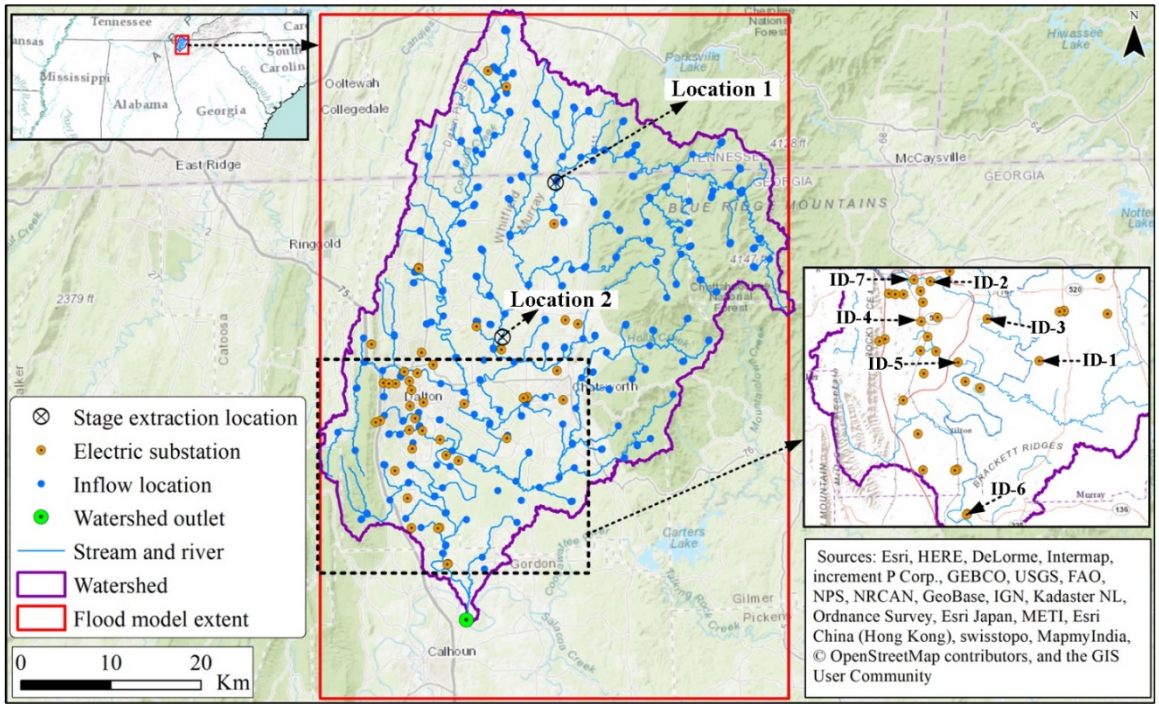

Figure 1. Conasauga River Watershed study area location, model extent, electric substations, and inflow locations. Background layer source: © OpenStreetMap contributors 2020. Distributed under a Creative Commons BY-SA License.

2.2. Streamflow Projections

The ensemble streamflow projections were generated by a hierarchical modeling framework, which started with regional climate downscaling followed by hydrologic modeling (Gangrade et al., 2020). The climate projections were generated by dynamically downscaling of 11 GCMs from the Coupled Model Intercomparison Project Phase-5 (CMIP5) data archive. Each GCM was used as lateral and lower boundary forcing in a regional climate model RegCM4 (Giorgi et al., 2012) at a horizontal grid spacing of 18

196 km over a domain that covered continental US and parts of Canada and Mexico (Ashfaq
197 et al., 2016) (Table 1). Each RegCM4 integration covered 40 years in the historic period
198 (1966–2005; hereafter baseline) and another 40 years in the future period (2011–2050)
199 under Representative Concentration Pathway 8.5 (RCP 8.5) emission scenario, with a
200 combined 880 years of data across all RegCM4 simulations. To capture the multi-decadal
201 climate variability, a minimum of 30-year period has been used in many studies (e.g.,
202 Alfieri et al., 2015a, 2015b). Given the additional data available from Gangrade et al.
203 (2020), we have adopted a longer 40-year period that may further enlarge the sample
204 space to better support the statistical analyses in this study.
205

206 Table 1. Summary of the 11 dynamically downscaled climate models (adopted from
207 Ashfaq et al., 2016).

S. No.	Climate model name	Number of flood events per climate model	Time period	
1	ACCESS1-0	40	1966–2005 (Baseline)	2011-2050 (Future/RCP 8.5)
2	BCC-CSM1-1			
3	CCSM4			
4	CMCC-CM			
5	FGOALS-g2			
6	GFDL-ESM2M			
7	MIROC5			
8	MPI-ESM-MR			
9	MRI-CGCM3			
10	NorESM1-M			
11	IPSL-CM5A-LR			

208

209 The RegCM4 simulated daily precipitation and temperature were further statistically
210 bias-corrected to a spatial resolution of 4 km following a quantile mapping technique,
211 described in Ashfaq et al. (2010, 2013). The 4 km Parameter-elevation Regressions on
212 Independent Slopes Model (PRISM; Daly et al., 2008) data was used as the historic
213 observations to support bias-correction. In the baseline period, the simulated quantiles of
214 precipitation and temperature were corrected by mapping them onto the observed
215 quantiles. In the future period, the monthly quantile shifts were calculated based on the
216 simulated baseline and future quantiles which were subsequently added to the bias
217 corrected baseline quantiles to generate bias-corrected monthly future data. Finally, the
218 monthly bias-corrections were distributed to the daily values while preserving in each
219 time period. This approach substantially improves the biases in the modeled daily
220 precipitation and temperature while preserving the simulated climate change signal.
221 Further details of the bias-correction are provided in Ashfaq et al. (2010, 2013) while the
222 information regarding the RegCM4 configuration, evaluation and future climate
223 projections are detailed in Ashfaq et al. (2016).
224 The hydrologic simulations were then conducted using the Distributed Hydrology
225 Soil Vegetation Model (DHSVM; Wigmosta et al., 1994), which is a process-based high-
226 resolution hydrologic model that can capture heterogeneous watershed processes and
227 meteorology at a fine resolution. DHSVM uses spatially distributed parameters, including
228 topography, soil types, soil depths, and vegetation types. The input meteorological data
229 includes precipitation, incoming shortwave and longwave radiation, relative humidity, air
230 temperature and wind speed (Wigmosta et al., 1994; Storck et al., 1998; Wigmosta et al.,
231 2002). The DHSVM performance and applicability has been reported in various earlier

232 climate and flood related studies (Elsner et al., 2010; Hou et al., 2019; Gangrade et al.,
233 2018, 2019, 2020). A calibrated DHSVM implementation from Gangrade et al. (2018) at
234 90 m grid spacing was used to produce 3-hourly streamflow projections using the
235 RegCM4 meteorological forcings described in the previous section (Table 1). In addition,
236 a control simulation driven by 1981–2012 Daymet meteorologic forcings (Thornton et
237 al., 1997) was conducted for model evaluation and validation. The hydrologic simulations
238 used in this study are a part of a larger hydroclimate assessment effort for the ACT River
239 Basin, as detailed in Gangrade et al. (2020). Since there is no major reservoir in the
240 CRW, the additional reservoir operation module (Zhao et al., 2016) was not needed in
241 this study.

242 Note that while the ensemble streamflow projections based on dynamical
243 downscaling and high-resolution hydrologic modeling from Gangrade et al. (2020) are
244 suitable to explore extreme hydrologic events in this study, they do not represent the full
245 range of possible future scenarios. Additional factors such as other GCMs, RCP
246 scenarios, downscaling approaches, and hydrologic models and parameterization may
247 also affect future streamflow projections. In other words, although these ensemble
248 streamflow projections can tell us how likely the future streamflow magnitude may
249 change from the baseline level, they are not the absolute prediction into the future. In
250 practice, these modeling choices will likely be study-specific based on the agreement
251 among key stakeholders. It is also noted that the new Coupled Model Intercomparison
252 Project Phase-6 (CMIP6) data have also become available to update the ensemble
253 streamflow projections, but is not pursued in this study.

254 **2.3. Inundation Modeling**

255 The ensemble inundation modeling was performed using TRITON, which is a
256 computationally enhanced version of Flood2D-GPU (Kalyanapu et al., 2011). TRITON
257 allows parallel computing using multiple graphics processing units (GPUs) through a
258 hybrid Message Passing Interface (MPI) and Compute Unified Device Architecture
259 (CUDA) (Morales-Hernández et al., 2021). TRITON solves the nonlinear hyperbolic
260 shallow water equations using an explicit upwind finite-volume scheme, based on Roe's
261 linearization. The shallow water equations are a simplified version of the Navier-Stokes
262 equations in which the horizontal momentum and continuity equations are integrated in
263 the vertical direction (see Morales-Hernández et al., (2021), for further model details). An
264 evaluation of TRITON performance for the CRW is presented and discussed in Section
265 3.3.
266 TRITON's input data includes digital elevation model (DEM), surface roughness,
267 initial depths, flow hydrographs, and inflow source locations (Kalyanapu et al., 2011;
268 Marshall et al., 2018; Morales-Hernández et al., 2020; Morales-Hernández et al., 2021).
269 In this study, the hydraulic and geometric parameters from the flood model evaluation
270 section (Section 3.3) were used in the flood simulation. The topography was represented
271 using the one-third arc-second (~10 m) spatial resolution DEM (Archuleta et al., 2017)
272 from the US Geological Survey (USGS). To improve the quality of the base DEM, as
273 discussed in the flood model evaluation section, the main channel elevation was reduced
274 by 0.15 m. Elevated roads and bridges that obstruct the flow of water were also removed.
275 For surface roughness, we used a single channel Manning's n value of 0.05 and a single
276 floodplain Manning's n value of 0.35. The selection of channel and floodplain Manning's
277 n value was based on the Whitfield County Flood Insurance Study (FIS, 2007), which

reported a range of Manning's n values estimated from field observations and engineering judgment for about 15 streams inside the CRW (section 3.2). Furthermore, a water depth value of 0.35 m was defined for the main river channel as an initial boundary condition. The zero velocity gradients were used as the downstream boundary condition. Further discussion of model parameter sensitivity and model evaluation are provided in sections 3.2 and 3.3.

The simulated DHSVM streamflow was used to prepare inflow hydrographs for ensemble inundation modeling. To provide a large sample size for frequency analysis, we selected all annual maximum peak streamflow events (the maximum corresponded to the outlet of CRW [Figure 1]) from the 1981–2012 control simulation (32 years), the 1966–2005 baseline simulation (440 years; 40 years × 11 models), and the 2011–2050 future simulation (440 years; 40 years × 11 models), with a total of 912 events. For each annual maximum event, the 3-hour timestep, 10-day hydrographs (which capture the peak CRW outlet discharge) across all DHSVM river segments were summarized. Following a procedure similar to Gangrade et al. (2019), these streamflow hydrographs were converted to TRITON inputs at 300 inflow locations selected along the NHD+ river network in the CRW (Figure 1). The TRITON model extent, shown in Figure 1, has an approximate area of 3945 km^2 and includes ~44 million model grid cells (7976 rows × 5474 columns in a uniform structured mesh). The ensemble flood simulations resulted in gridded flood depth and velocity output at 30-minute intervals. The simulations generated an approximately 400 Terabyte data and utilized ~2000 node hours on the Summit supercomputer, managed by the Oak Ridge Leadership Computing Facility at Oak Ridge National Laboratory.

2.4. Flood Inundation Frequency Analysis

Given the nature of GCM experiments, each set of climate projections can be considered as a physics-based realization of historic and future climate under specified emission scenarios. Therefore, an ensemble of multimodel simulations can effectively increase the data lengths and sample sizes that are keys to support frequency analysis, especially for low-AEP events. In this study, we conducted flood frequency analyses separately for the 1966–2005 baseline and 2011–2050 future periods so that the difference between the two periods represent the changes in flood risk due to climate change.

To prepare the flood frequency analysis, we first calculated the maximum flood depth at every grid in each simulation. A minimum threshold of 10 cm flood depth was used to judge whether a cell was wet or dry (Gangrade et al., 2019). Further, for a given grid cell, if the total number of non-zero flood depth values (i.e., of the 440 depth values) was less than 30, the grid cell was also considered dry. This threshold was selected based on the minimum sample size requirement for flood depth frequency analysis suggested by Li et al. (2018). Next, we calculated the maximum flooded area (hereafter used alternatively with "floodplain area") for each simulation. A log-Pearson Type III (LP3) distribution was then used for frequency analysis following the guidelines outlined in Bulletins 17B (USGS, 1982; Burkey, 2009) and 17C (England Jr. et al., 2019). Two types of LP3 fitting were performed. The first type of fitting is event-based that fitted LP3 on the maximum inundation area across all ensemble members. The second type of fitting is grid-based (more computationally intensive) that fitted LP3 on the maximum flood depth at each grid cell across all ensemble members. For both types of fittings, the frequency estimates

at 4%, 2%, 1%, and 0.5% AEP (corresponding to 25-, 50-, 100-, and 200-year return levels) were derived for further analysis.

It is also noted that in addition to the annual maximum event approach used in this study, one may also use the peak-over-threshold (POT) approach which can select multiple streamflow events in a very wet year. While such an approach can lead to higher extreme streamflow and inundation estimates, the timing of POT samples is fully governed by the occurrences of wet years. In other words, if the trend of extreme streamflow is significant in the future period, the POT samples will likely occur more in the far future period. We hence select the annual maximum event approach that can sample maximum streamflow events more evenly in time, which can better capture the evolution of extreme events with time under the influence of climate change.

2.5. Vulnerability of Electricity Infrastructure

The vulnerability of electricity infrastructures to climate change-induced flooding was evaluated using the ensemble flood inundation results. The 44 electric substations (Figure 1) collected from the publicly available Homeland Infrastructure Foundation-Level Data (HIFLD, 2019) were considered to be the electrical components susceptible to flooding. To evaluate the vulnerability of these substations, we overlapped the maximum flood extent from each ensemble member with all substations to identify the substations that might be inundated under the baseline and future climate conditions. Further, as an additional flood hazard indicator, the duration of inundation was estimated at each of the affected substations using the ensemble flood simulation results.

The vulnerability analysis was performed for two different flood mitigation scenarios. In the first scenario, we assumed that no flood protection measures were provided at all

347 substations. Hence, the substations that intersected with the flood footprint were
348 considered to be failed. In the second scenario, it was assumed that flood protection
349 measures were adopted for all substations following the FEMA P-1019 recommendation
350 (FEMA, 2014). According to FEMA P-1019 (FEMA, 2014), for emergency power
351 systems within critical facilities, the highest elevation among (1) the base flood elevation
352 (BFE: 1% FEMA AEP flood elevation) plus 3 feet (~0.91 m), (2) the locally adopted
353 design flood elevation, and (3) the 500-year flood elevation can be used to design flood
354 protection measures. Since the three recommended elevations were not available at all
355 substation locations, we focused only on the BFE plus ~0.91 m option. In addition, since
356 in the CRW the majority of existing flood insurance maps were classified as Zone A—
357 meaning that the special flood hazard areas were determined by approximate methods
358 without BFE values (FEMA, 2002)—we used the maximum flood depth values across all
359 control simulation years as the BFE values in this second mitigation scenario.

360 During the vulnerability analysis, we also assumed that (1) the one-third arc-second
361 spatial resolution DEM might reasonably represent the elevation of substations, (2)
362 existing substations would remain functional and would not be relocated, and (3) no
363 additional hardening measures (i.e., protections such as levees, berms, anchors, and
364 housings) will be adopted in the future period. Also, the cascading failure of a substation
365 due to grid interconnection was not considered in this study.

366

367 **3. Results and Discussion**

368 **3.1. Streamflow Projections**

369 This section presents a comparison of the annual maximum peak streamflow (at the
370 outlet of CRW) used in the control, baseline, and future simulations. The sample size
371 included 32 events from the control (1981–2012) simulation, 440 events from the
372 baseline (1966–2005) simulations, and another 440 events from the future (2011–2050)
373 simulations. These samples are illustrated in box and whisker plots in Figure 2, where
374 central mark indicate the median, while bottom and top edges indicate the 25^{th} and 75^{th}
375 percentiles respectively. The whiskers extend to the furthest data points not considered
376 outliers, which correspond to approximately ± 2.7 standard deviations and 99.3%
377 coverage if the data are normally distributed. As is evident from Figure 2, the
378 distributions of annual maximum peak streamflow values in the control and baseline
379 simulations are comparable. The upper and lower whiskers in the control simulation are
380 727.6 m^3/s and 84.2 m^3/s, which compare well to the 722.5 m^3/s and 65.2 m^3/s values in
381 the baseline simulation. In addition, we also conducted a two-tailed two-sample t-test (α
382 = 0.05) to compare if the means of control and baseline annual maximum streamflow are
383 statistically different. The results yielded a p-value of 0.09 which suggested that there is
384 no significant difference between the means of both control and baseline simulations. A
385 larger number of outliers are present in the baseline simulation, which is due to the larger
386 sample size (440 versus 32).
387 Under the future projection, an increase in the maximum peak streamflow is shown,
388 where the upper whisker in the future projection is ~21% higher than the baseline.
389 Moreover, the maximum of distribution in the future climate (2036.7 m^3/s) is also much
390 higher than that in the baseline climate (1436.7 m^3/s), suggesting a higher future flood

risk in the CRW. The increasing trend of streamflow extremes in the CRW is consistent with the overall findings in the ACT River Basin (Gangrade et al., 2020).

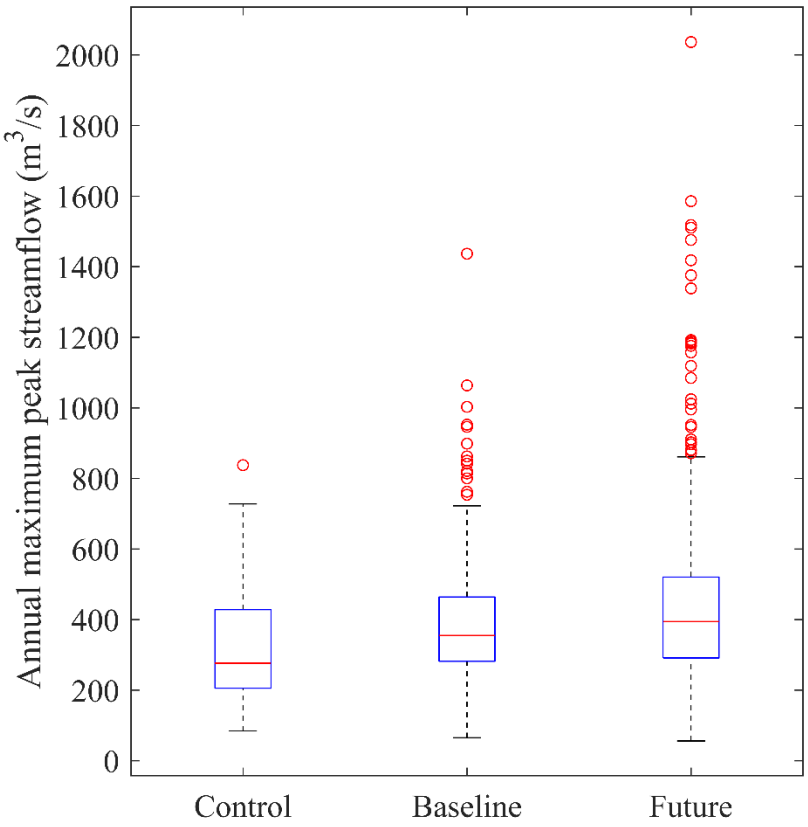

Figure 2. A comparison of annual maximum peak streamflow at the outlet of Conasauga River Watershed. The sample size includes 32 events from the control (1981–2012), 440 from the baseline (1966–2005), and another 440 from the future (2011–2050) periods.

3.2. Sensitivity Analysis for Flood Model

For a better understanding and selection of suitable TRITON parameters, a series of sensitivity analyses were conducted using different combinations of Manning's roughness, initial water depths, and river bathymetry correction factors (Table 2).

Table 2. Summary of hydraulic and geometric parameters used in the sensitivity analysis.

Sensitivity parameter	Scenario	Initial water depth values (m)	Surface roughness (Manning's n values)	Bathymetry correction factor (m)
Initial water depth	1	0.00	n_{ch} =0.050 / n_{fldpl} =0.350	-0.15
	2	0.15		
	3	0.35		
	4	0.45		
	5	0.55		
	6	0.65		
Surface roughness	1	0.35	N_1: n_{ch} =0.035 / n_{fldpl} =0.06	-0.15
	2		N_2: n_{ch} =0.040 / n_{fldpl} =0.25	
	3		N_3: n_{ch} =0.045 / n_{fldpl} =0.30	
	4		N_4: n_{ch} =0.050 / n_{fldpl} =0.35	
	5		N_5: n_{ch} =0.055 / n_{fldpl} =0.45	
	6		N_6: n_{ch} =0.060 / n_{fldpl} =0.50	
Bathymetry correction factor	1	0.35	n_{ch} =0.050 / n_{fldpl} =0.350	0.00
	2			-0.15
	3			-0.45
	4			-0.75
	5			-1.00
	6			-1.25

Note: n_{ch} represents the Manning's n value in the main channel and n_{fldpl} represents the Manning's n value in the floodplain areas.

In calibrating a hydraulic model, it is a common practice to adjust the estimated Manning's n value, as it is the most uncertain and variable input hydraulic parameter (Brunner et al., 2016). In this study, we tested six different scenarios (Table 2) based on the Whitfield County Flood Insurance Study (FIS, 2007), which reported a range of Manning's n values estimated from field observations and engineering judgment for about 15 streams inside the CRW. It is noted that the depth variation of Manning's roughness is not considered in the current study. Readers are referred to studies such as

Saksena et al. (2020) for additional information on the dynamic Manning's roughness for potential hydrology and hydraulics applications.

To establish an initial condition for TRITON, a sensitivity analysis was performed on selected initial water depth values (ranging from 0 m to 0.65 m, Table 2) to understand their relative effects. To select ranges for the initial water depth, we summarized the observed water depth values that corresponds to low flow values at five USGS gauge stations inside the CRW. The distribution of observed water depth values from the five gauges showed average values ranging from 0.25 to 0.65m. Existing DEM products, even those with high spatial resolution (i.e., 10 m or finer), do not represent the elevation of river bathymetry accurately (Bhuyian et al., 2014). For the CRW, Bhuyian et al. (2019) found that the one-third arc-second spatial resolution base DEM over-predicted the inundation extent because of the bathymetric error, which reduced the channel conveyance. In this study, we tested various bathymetry correction factors (ranging from −1.25 m to 0 m, Table 2) by reducing the DEM elevation along the main channel to understand the sensitivity of TRITON.

The sensitivity analysis was performed using the February 13–22, 1990 flood event that has the maximum discharge among all 32 control simulation events. To evaluate relative sensitivity of TRITON, we extracted simulated flood depths at two arbitrary selected locations (Figure 1) and estimated the relative inundation area differences. The impacts of initial water depths were significant only at the beginning where low flow values dominated the hydrographs (Figure 3a, 3d). Larger initial water depth values generated higher flood inundation depths for both sample locations. Although the differences in flood inundation extents relative to the dry bed show an increasing trend,

438 the relative differences are less than 1.4% (Figure 4a). Increase in the channel and
439 floodplain Manning's n values resulted in higher flood depths for both sample locations
440 (Figure 3b and 3e). The relative flood inundation area differences increase from about
441 23% to 31% (Figure 4b) when the channel and floodplain Manning's n values are
442 increased from 0.035 to 0.06 and from 0.06 to 0. 50, respectively. Reduction in the
443 elevation of river bathymetry (to improve the quality of the base DEM) results in a direct
444 increase in maximum flood depth due to change in the river conveyance (Figure 3c and
445 3f). It also results in a decrease in the maximum flood extent (Figure 4c), as more water
446 is allowed to transport through the main channel instead of the floodplain. A similar
447 phenomenon was observed in other studies including Dey et al., (2019).Overall, the
448 results showed that TRITON was more sensitive to the Manning's n values than the
449 initial water depths and bathymetric correction factors.

450

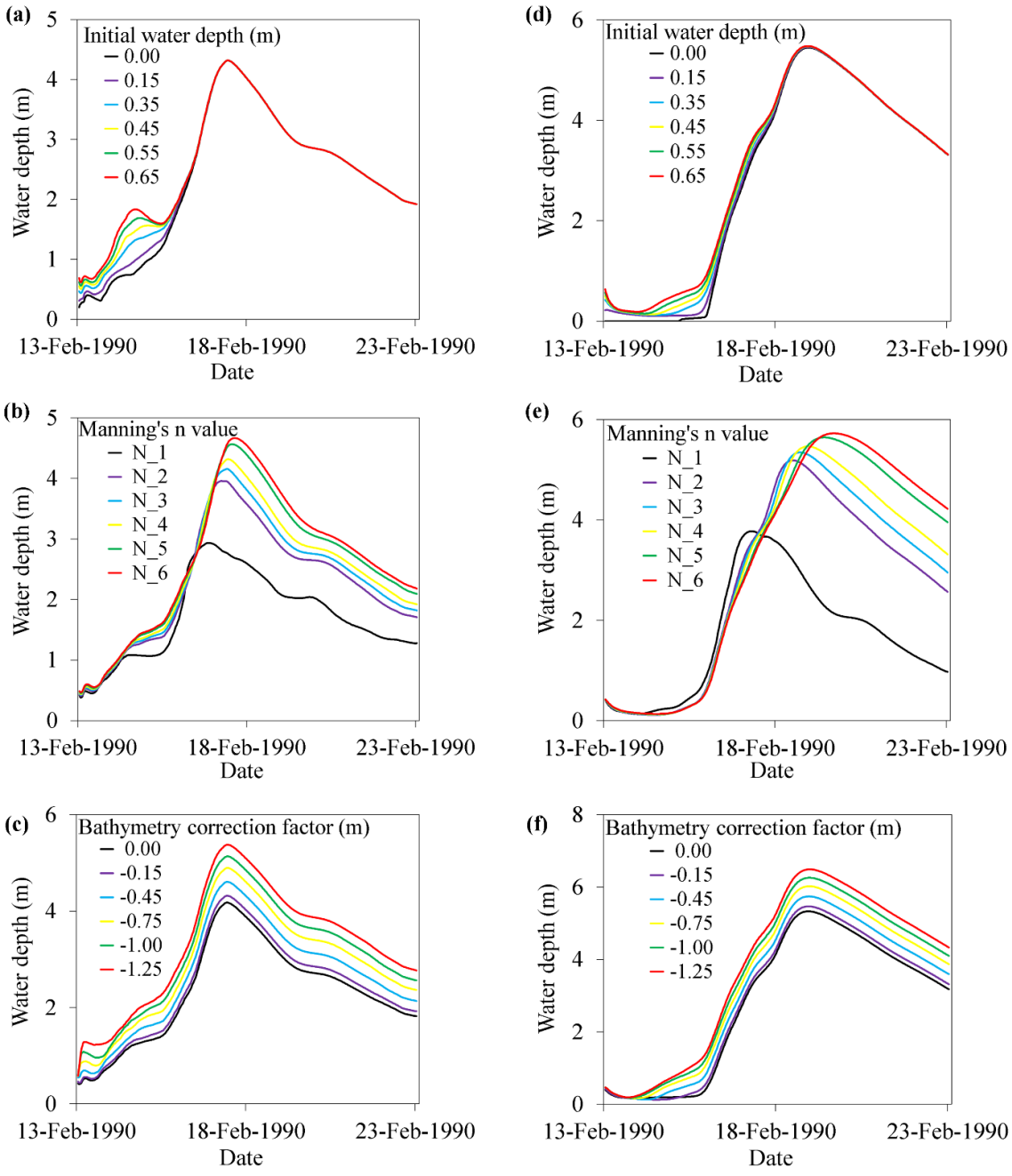

451

452 Figure 3. Simulated flood inundation depths extracted at location 1 (a, b, c) and at

453 location 2 (d, e, f). Note: Location 1 and 2 are shown in Figure 1. A description of the

454 Manning's n values (N_1 to N_6) can be found in Table 2.

455

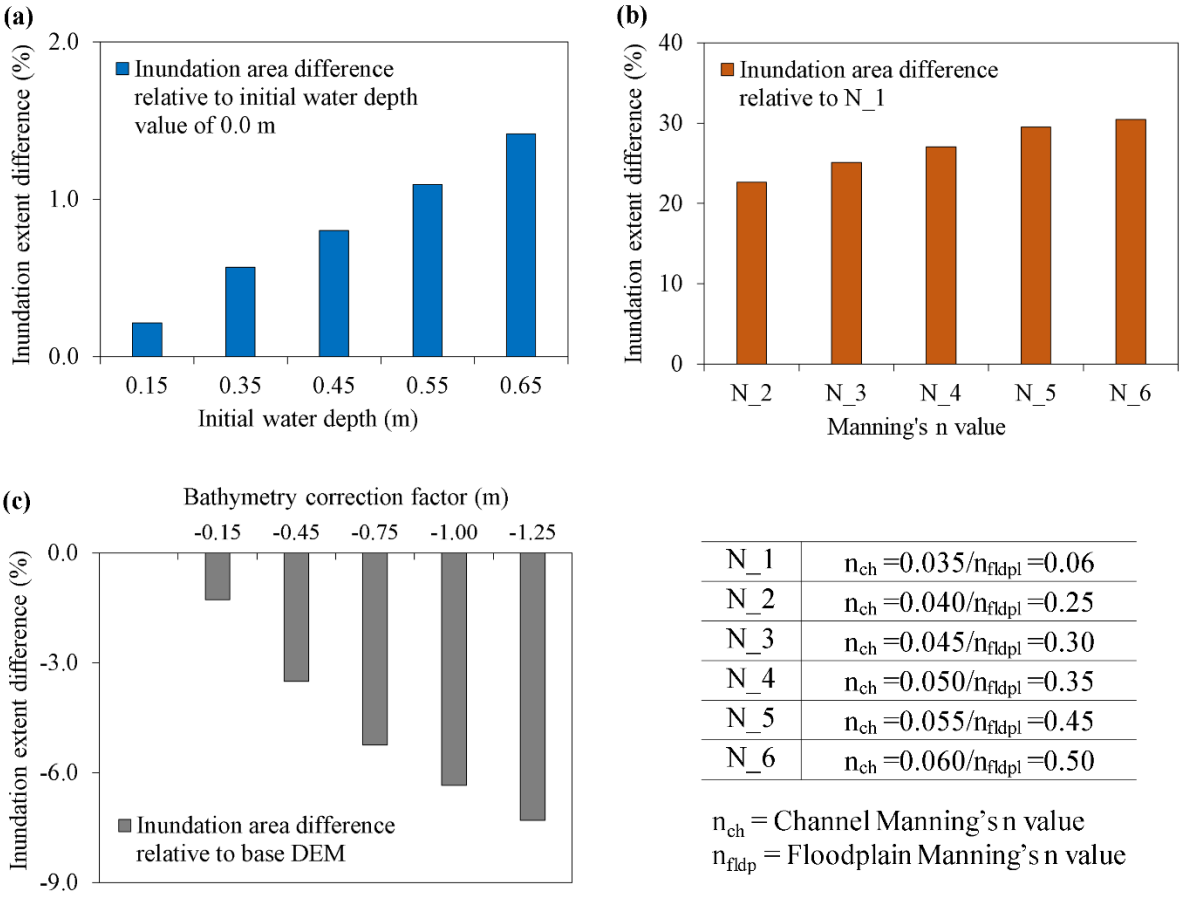

N_1	n_{ch} =0.035/n_{fldpl} =0.06
N_2	n_{ch} =0.040/n_{fldpl} =0.25
N_3	n_{ch} =0.045/n_{fldpl} =0.30
N_4	n_{ch} =0.050/n_{fldpl} =0.35
N_5	n_{ch} =0.055/n_{fldpl} =0.45
N_6	n_{ch} =0.060/n_{fldpl} =0.50

n_{ch} = Channel Manning's n value
n_{fldp} = Floodplain Manning's n value

Figure 4. Change in simulated maximum flood inundation extents for (a) initial water depth, (b) Manning's n value, and (c) bathymetry correction factor.

3.3. Flood Model Evaluation

Because of a lack of observed streamflow data in the CRW, the performance of TRITON was evaluated by comparing the simulated 1% AEP flood map with the published 1% AEP flood map from FEMA (FEMA, 2019). The purpose of this assessment is to understand whether TRITON can provide comparable results to the widely accepted FEMA flood estimates. While the FEMA AEP flood maps do not necessarily represent complete ground truth, such a comparison is the best option given

467 the data challenge. Similar approach has been utilized by several previous studies in the
468 evaluation of large-scale flood inundation evaluation (Alfieri et al., 2014; Wing et al.,
469 2017; Zheng et al., 2018; Gangrade et al., 2019).

470 To derive the 1% AEP flood map using TRITON, the ensemble-based approach used
471 by Gangrade et al. (2019) was followed. The assessment started by preparing the
472 streamflow hydrographs used to construct the 1% AEP flood map. The 1981–2012
473 annual maximum peak events and their corresponding 10-day streamflow hydrographs
474 were extracted from the control simulation. These streamflow hydrographs were then
475 proportionally rescaled to match the 1% AEP peak discharge estimated at the watershed
476 outlet (Figure 1), following the frequency analysis procedures outlined in Bulletin 17C
477 (England Jr. et al., 2019). The streamflow hydrographs from control simulations were
478 used for the peak discharge frequency analysis.

479 The results reported in the sensitivity analysis were also used to help identify suitable
480 TRITON parameters. In addition to streamflow hydrographs, TRITON requires DEM,
481 initial water depth, and Manning's n value. To minimize the effect of bathymetric error in
482 the base DEM (Bhuyian et al., 2014; Bhuyian et al., 2019), we reduced the elevation
483 along the main channel by 0.15 m (i.e., a bathymetry correction factor). Although this
484 simple approach is unlikely to adjust the channel bathymetry to its true values, it can
485 improve the channel conveyance volume that is lost in the base DEM. To further improve
486 the quality of the base DEM, we removed elevated roads and bridges that could obstruct
487 the flow of water in some of the streams and rivers. An initial water depth of 0.35 m was
488 also selected in this study. For the surface roughness, a couple of flood simulations were
489 performed by adjusting the Manning's n values for the main channel and floodplain to

490 achieve satisfactory agreement between the simulated and the reference FEMA flood
491 map. We eventually selected a single channel Manning's n value of 0.05 and a single
492 floodplain Manning's n value of 0.35.

493 Three evaluation metrics, including fit, omission, and commission (Kalyanapu et al.,
494 2011) were used to quantify the differences between the modeled and reference flood
495 map. The measure of fit determines the degree of relationship, while the omission and
496 commission statistically compare the simulated and reference FEMA flood maps
497 (Kalyanapu et al., 2011). The comparison between the simulated maximum inundation
498 and the corresponding 1% AEP FEMA flood map showed 80.65% fit, 5.52%
499 commission, and 15.36% omission (Figure 5), demonstrating that the TRITON could
500 reasonably estimate flood inundation extent, and depths in the CRW. The computational
501 efficiency of TRITON can further support ensemble inundation modeling to provide
502 additional variability information that cannot be provided by the conventional
503 deterministic flood map.

504 Although we have obtained satisfactory model performance for the purpose of our
505 study, the flood model implementation has some limitations that may be enhanced in
506 future studies. They include:

507 • Spatially varying Manning's n values may be derived based on high-resolution
508 land use land cover (LULC) conditions to better represent the spatial
509 heterogeneity in the modeling domain.

510 • Apart from changes in future runoff and streamflow, projections of future LULC
511 and its corresponding surface roughness can be considered to understand the
512 broader impacts due to environment change.

- In this study, we corrected DEM bias along the river channel cells by simplified bathymetry correction factors. More sophisticated bathymetric configuration (i.e., channel shape and sinuosity) can be considered to better represent channel conveyance.
- The current TRITON model does not provide capability to route local runoff and external inflows through stormwater drainage systems. Coupling with additional stormwater drainage models can be a potential future direction.
- Hydraulic and civil structures such as bridges, culverts, and weirs have not been included since TRITON does not provide for the modeling of such components. This can affect the accuracy of the flood depths, velocities, and flood extents around these structures.

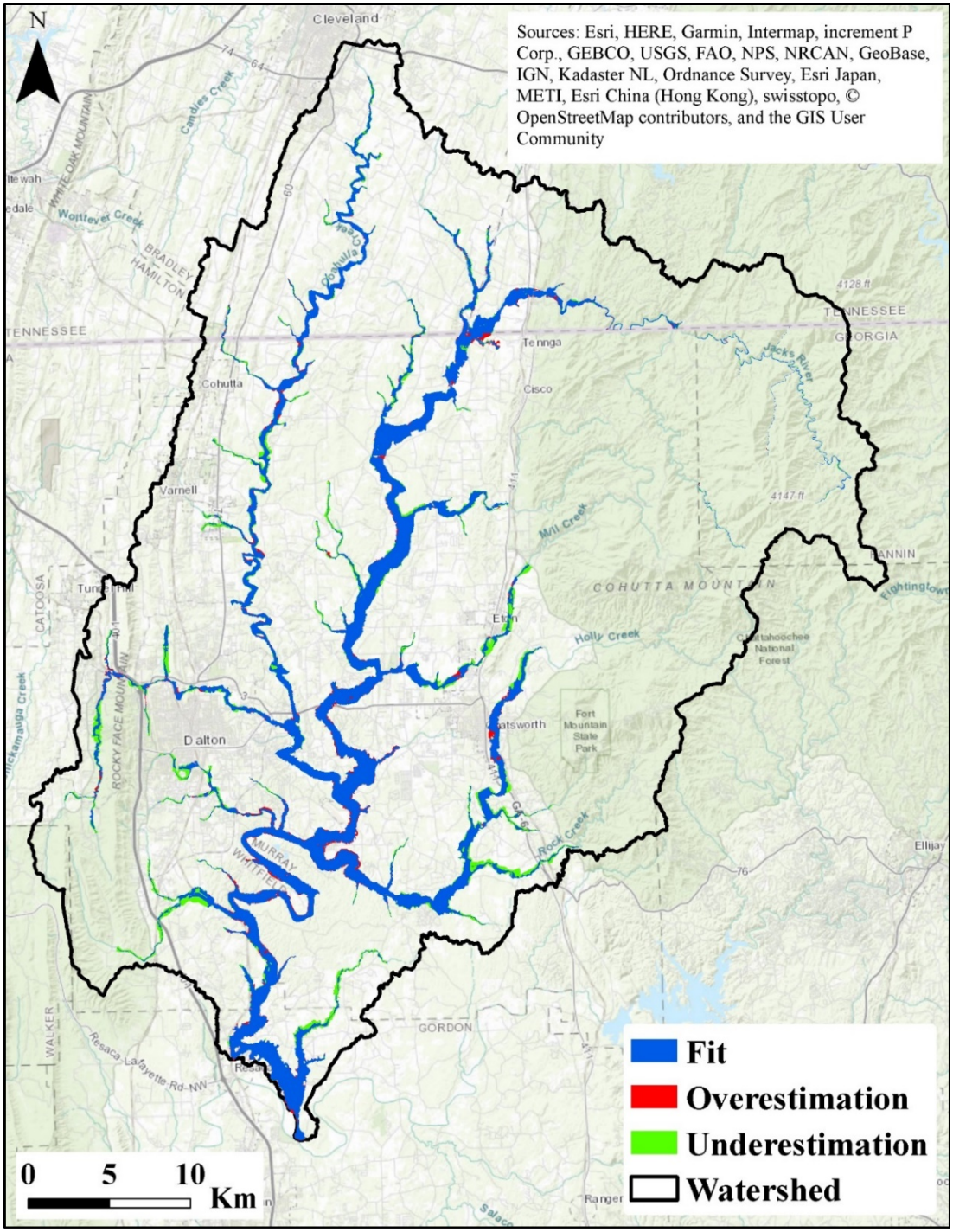

525

526 Figure 5. Comparison of simulated maximum flood extent with the corresponding FEMA

527 1% AEP flood map for the Conasauga River Watershed. Background layer source: ©

528 OpenStreetMap contributors 2020. Distributed under a Creative Commons BY-SA

529 License.

530

531 **3.4. Change in Flood Regime**

532 In this section, the projected changes in flood regime were calculated using the
533 flooded area from the baseline and future simulations for each ensemble member. Figure
534 6 illustrates the box and whisker plots for each of the 11 dynamically downscaled GCMs.
535 Given the small sample size in each distribution (40 compared to 440 in Figure 2), the
536 whiskers extend the largest/smallest data points with no outlier detection. For 9 out of the
537 11 downscaled climate models, the mean of 40 flood inundation showed an increase in
538 the floodplain area in the future period. In terms of the 75^{th} percentile and maximum, 10
539 out of 11 models showed increase in the floodplain area. The distribution of maximum
540 future inundation of 4 models are found to be statistically different than their baseline
541 distributions at a 5% significance level. Note that the spread in the future period is
542 generally larger than the spread in the baseline period, suggesting an increase in the
543 hydrologic variability in the future period. Also, while the results from different models
544 were generally consistent, some inter-model differences were noted, which highlight the
545 need of a multi-model framework to capture the uncertainty in the future climate
546 projections. The multi-model approach provides a range of possible flood inundation
547 extents, which is critical for floodplain management decision making. The potential
548 increase in the floodplain area also demonstrates the importance of incorporating climate
549 change projections in the floodplain management regulations.

550

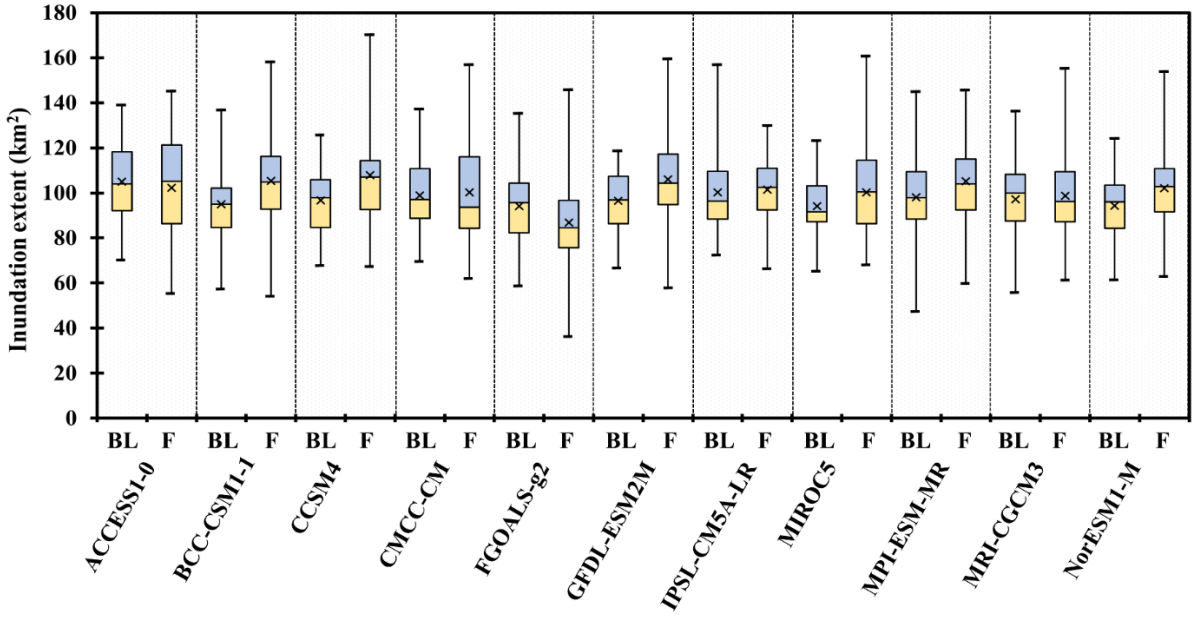

Figure 6. A summary of simulated maximum flood inundation extents obtained from the baseline and future scenarios. The mean flooded area values are shown by × symbols. Note: The suffix "_BL" represents baseline scenarios and the suffix "_F" represents future scenarios.

3.5. Flood Inundation Frequency Curve and Map

Figure 7 shows the relationship between the 440 flooded area values (across 11 downscaled GCMs) and their corresponding peak streamflow at the watershed outlet, for both the baseline and future periods. Overall, both results (Figure 7a and 7b) exhibit strong nonlinear relationships with high R^2 values. The results suggest that peak streamflow is a significant variable controlling the total flooded area, but the variability of flooded area could not be explained by peak streamflow alone. For instance, in the baseline period, the peak streamflow values of 423.63 m^3/sec and 424.25 m^3/sec correspond to 106.85 km^2 and 94.89 km^2 floodplain areas, respectively (Figure 7a).

565 Similarly, in the future period, the peak streamflow values of 433.27 m^3/sec and 434.21

566 m^3/sec correspond to 110.76 km^2 and 99.26 km^2 floodplain areas (Figure 7b).

567

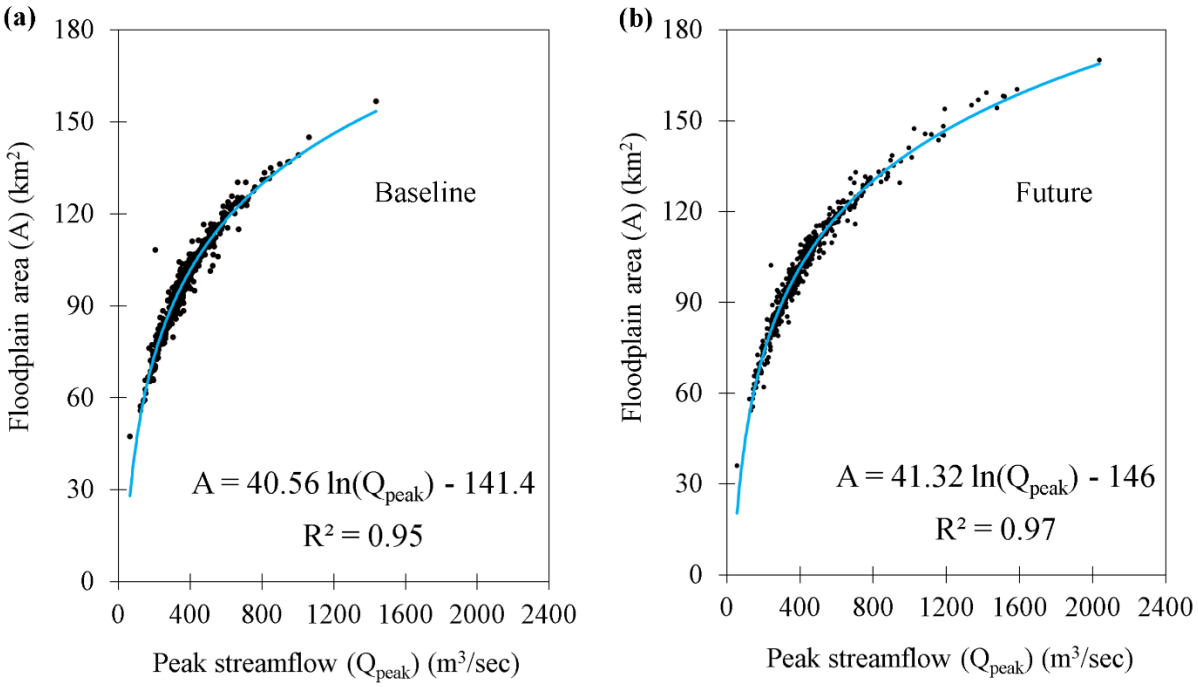

568

569 Figure 7. Relationship between floodplain areas and peak streamflow values at the

570 watershed outlet for (a) baseline and (b) future scenarios. The blue lines indicate the

571 logarithmic best-fit.

572

573 Figure 8 shows the event-based flood inundation frequency curves and their

574 corresponding 95% confidence intervals in both the baseline and future periods, for

575 which each frequency curve was derived using an ensemble of 440 years of data. The use

576 of long-term data helped reduce the uncertainty and add more confidence in the

577 evaluation of the lower AEP estimates. This type of assessment cannot be achieved using

578 only historic streamflow observations, for which the limited records present a major

challenge for lower AEP estimates. For most of the exceedance probabilities, the flooded areas projected an increase in the inundation areas in the future period when compared to the baseline period. The 1% AEP flood shows an ~16 km^2 increase in the inundation area (137.75 km^2 in the baseline period versus 153.43 km^2 in the future period) (Figure 8). Similar results can be observed in inundation frequency curves developed for other AEPs (not shown).

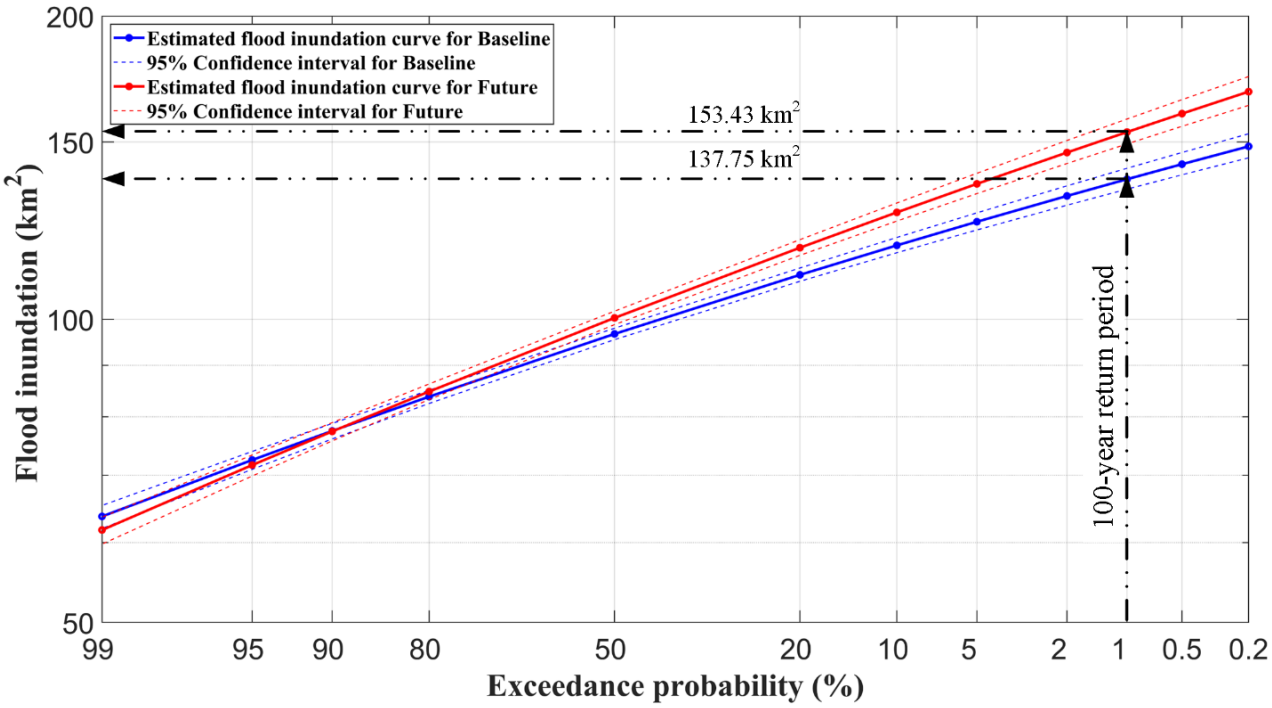

Figure 8. A summary of flood inundation frequency curves for the baseline and future periods.

The grid-based flood depth frequency results at 0.5%, 1%, 2%, and 4% AEP levels are illustrated in Figure 9. In each panel, the projected change (i.e., future minus baseline) at each grid is shown. The corresponding histogram across the entire study area is

593 presented in Figure 10. As mentioned in section 2.4, the LP3 distribution was used for
594 frequency analysis. In order to understand the suitability of LP3, we also conducted a
595 comparative analysis to test an alternative log-normal (LN) distribution. By using the
596 Anderson-Darling (Anderson and Darling, 1954) goodness-of-fit test ($\alpha = 0.05$) along
597 with the Akaike Information Criteria (Akaike, 1974), we found no substantial difference
598 between these two distributions (not showed), for the purpose of our application. It is
599 noted, however, that our goal in this study is not to identify the most suitable choice of
600 flood depth distribution. Therefore, other more suitable distributions may exist but this is
601 beyond the scope of this study.

602 Based on the comparisons in Figure 10, it is estimated that the flood depth values at
603 ~80% of grid cells would increase by 0.2 to 1.5 m due to projected changes in climate
604 (Figure 10). For 0.5% and 1% AEP flood depth frequency maps (Figure 9a and 9b), the
605 changes in flood depth were more pronounced in the lower part of the CRW, near the
606 City of Dalton (where there are large population settlements), thereby increasing the
607 likelihood of population exposure to flood risk in the future period. Furthermore, for the
608 1% flood depth frequency map (Figure 9b), the projected increase in flood depths and
609 spatial extent has the potential to extend the flood damage far beyond the FEMA's
610 current base floodplain area. Therefore, these results highlight the need for climate
611 change consideration in the floodplain mapping. The approach presented in this study can
612 provide an alternative floodplain delineation technique, as it can be applied to develop
613 flood depth frequency maps that are reflective of the future climate.

614

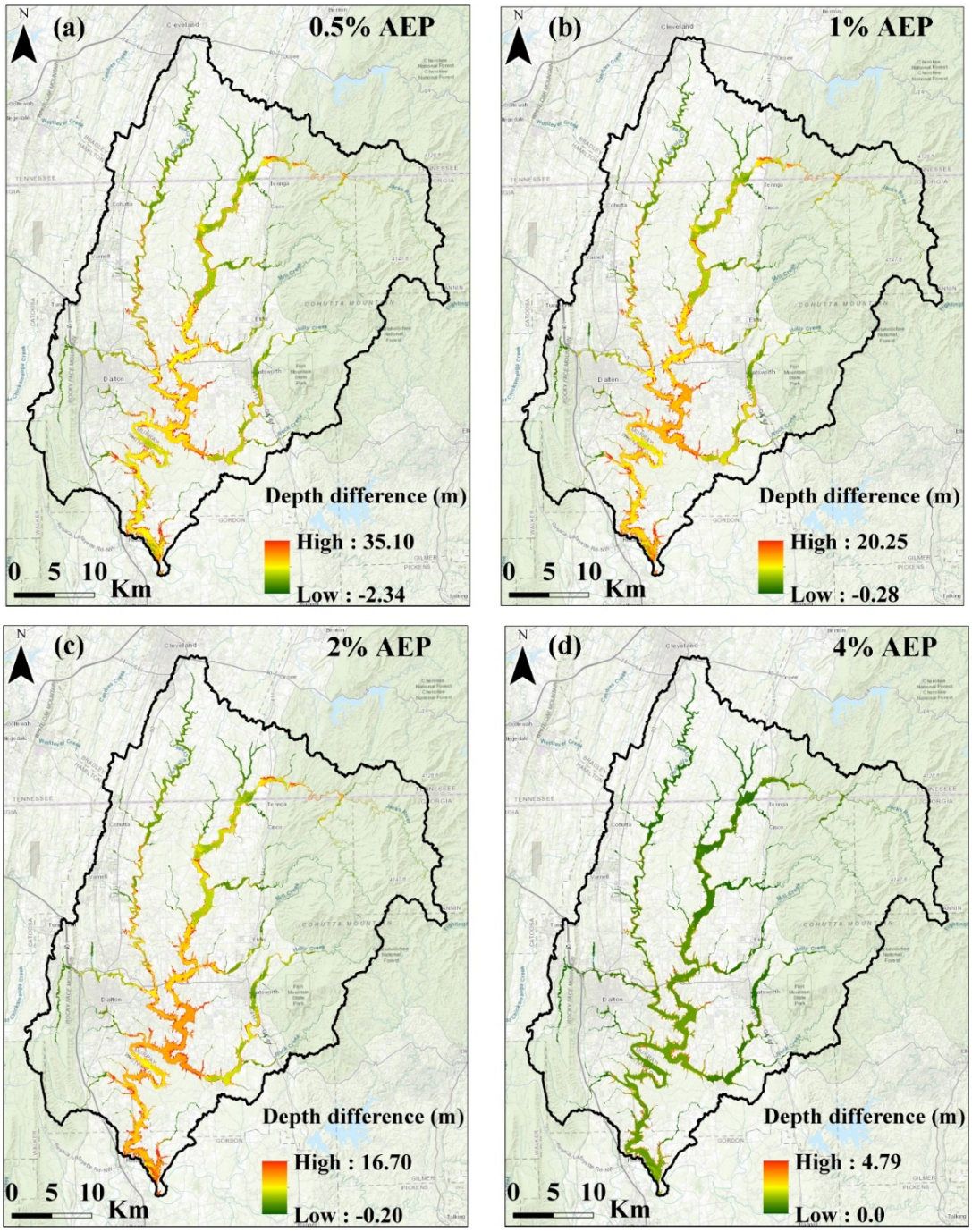

Figure 9. Projected change (future minus baseline period) in flood depth frequency maps for (a) 0.5%, (b) 1%, (c) 2%, and (d) 4% AEPs. ArcGIS background layer sources: ESRI, HERE, Garmin, Intermap, GEBCO, USGS, Food and Agriculture Organization, National Park Service, Natural Resources Canada, GeoBase, IGN, Kadaster NL, Ordnance Survey, METI, Esri Japan, Esri China, the GIS User Community, and © OpenStreetMap contributors 2020. Distributed under a Creative Commons BY-SA License.

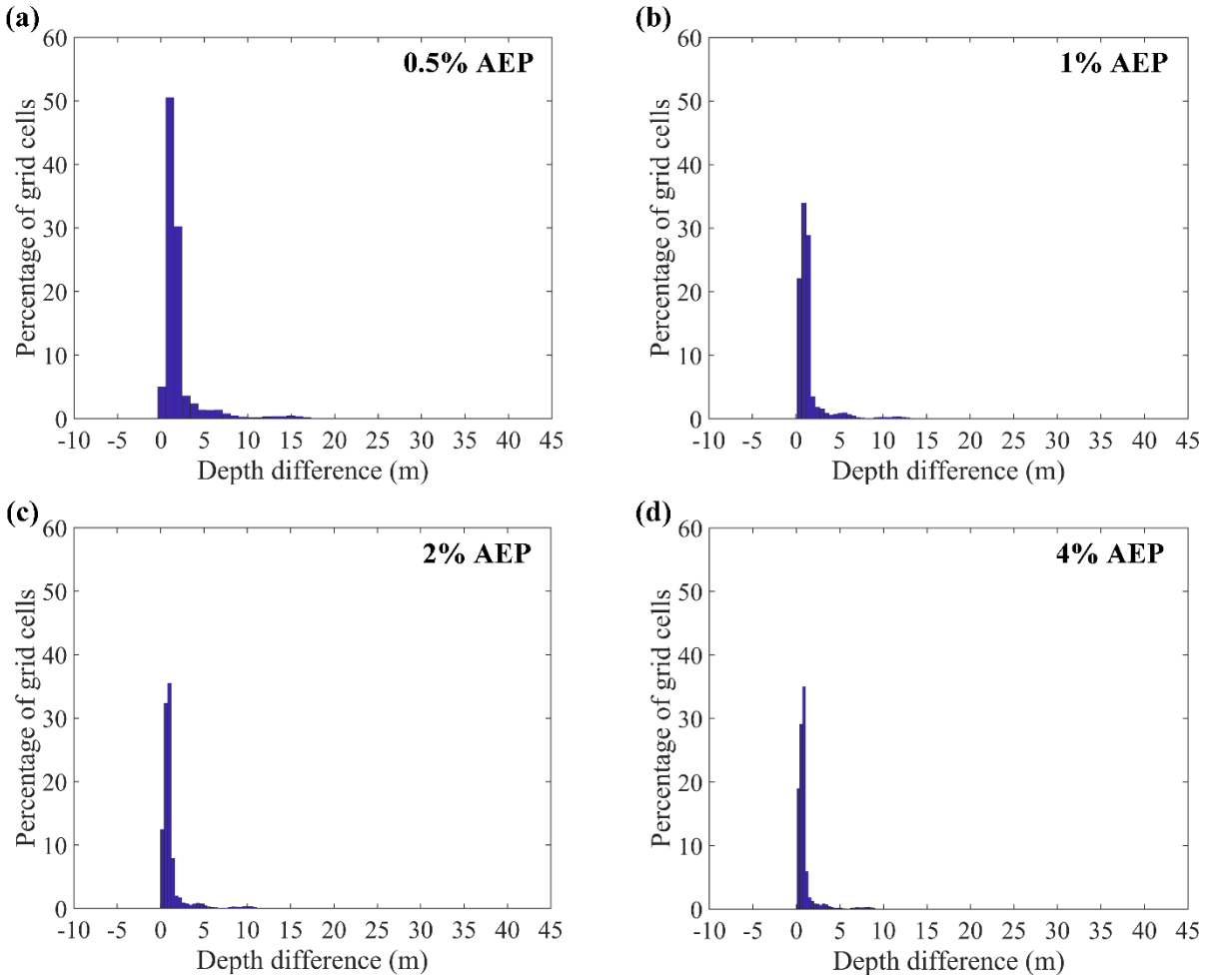

Figure 10. Histograms for the future changes (2011–2050) in the flood depth relative to the baseline period (1966–2005) for (a) 0.5%, (b) 1%, (c) 2%, and (d) 4% AEP flood depth frequency maps.

3.6. Vulnerability of Electricity Infrastructure

Figure 11a shows the box and whisker plot for the distributions of maximum flood depth values extracted at the substation location across all the baseline and future simulations, assuming that no flood protection measures were adopted (mitigation scenario 1). Of the 44 substations, 5 substations could have been affected during the

632 baseline period, while 7 substations are projected to be affected during the future period
633 (Figure 11a). Increases are indicated not only for the number of affected substations but
634 also for flood inundation depth values in the projected future climate. Overall, the mean
635 of the ensemble flood depth values shows an ~0.6 m increase in the future period (Figure
636 11a). Such an increase in the flood depth magnitude has the potential to exacerbate flood
637 related damage to electrical components, which can inflate the cost of hardening
638 measures such as elevating substations and constructing flood-protective barriers. As
639 expected, when the substations were flood-proofed up to BFE plus ~0.91 m (mitigation
640 scenario 2), the number of affected substations is reduced to three and four during the
641 baseline and future periods, respectively (Figure 11b). The locations of substations that
642 were impacted in the baseline period, in both mitigation scenarios, are consistent with the
643 Whitfield County Emergency Management Agency report map (EMA, 2016) that shows
644 the locations of critical facilities vulnerable to the historical flooding.

645 The maximum inundation durations at the affected substations are summarized in
646 Figure 12a (mitigation scenario 1) and Figure 12b (mitigation scenario 2). For both
647 mitigation scenarios and all affected substations, ensemble mean inundation durations
648 exhibited an increase under future climate condition. This increase in inundation duration
649 probably would render substations out of service for longer periods of time by making it
650 difficult to repair damaged substation equipment and restore grid services to customers.
651 The potential hazards and consequences may also extend to critical facilities that are
652 supplied by the affected substations. Similar to results presented in the previous sections,
653 these results demonstrate the need for improving existing flood mitigation measures by
654 incorporating the trends and uncertainties that originate from climate change. The

vulnerability analysis approach presented in this study will better equip floodplain managers to identify the most vulnerable substations and to recommend suitable adaptation measures, while allocating resources efficiently.

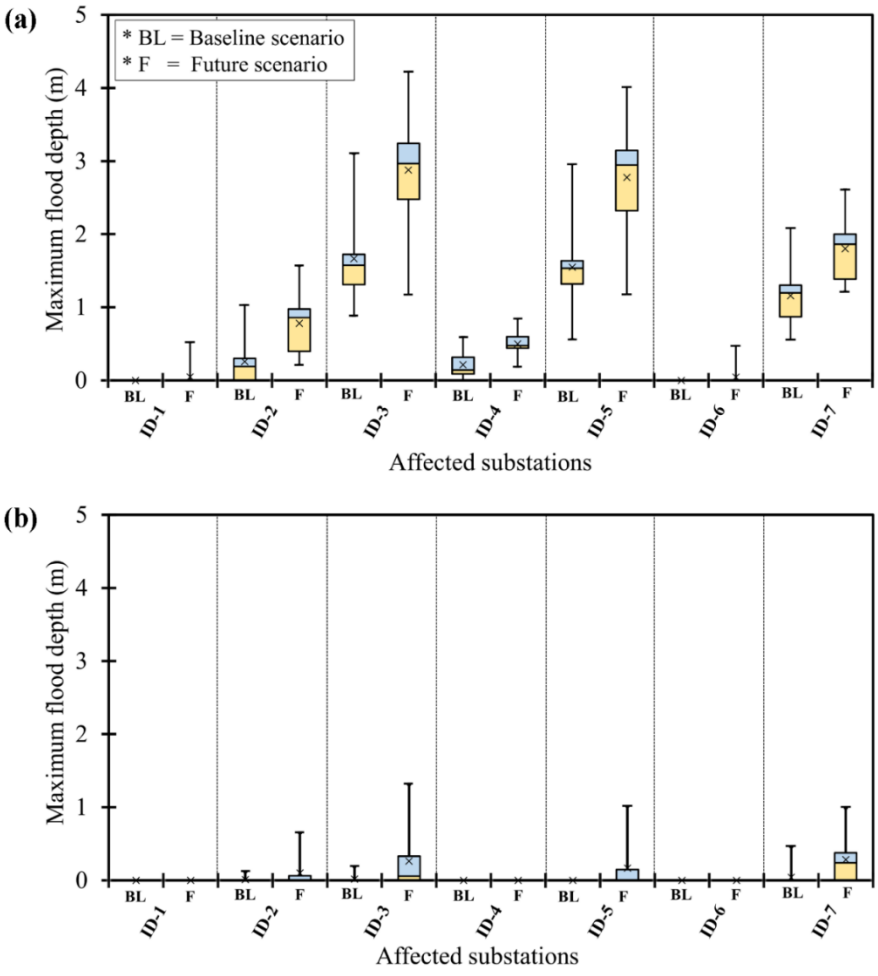

Figure 11. A summary of maximum flood depths for substations that were affected in the baseline and/or future periods (a) without flood protection measures and (b) with flood protection measures. Note: Affected substations with their corresponding IDs are shown in Figure 1. There are no negative values in the vertical axis, as the minimum flood depth value is zero.

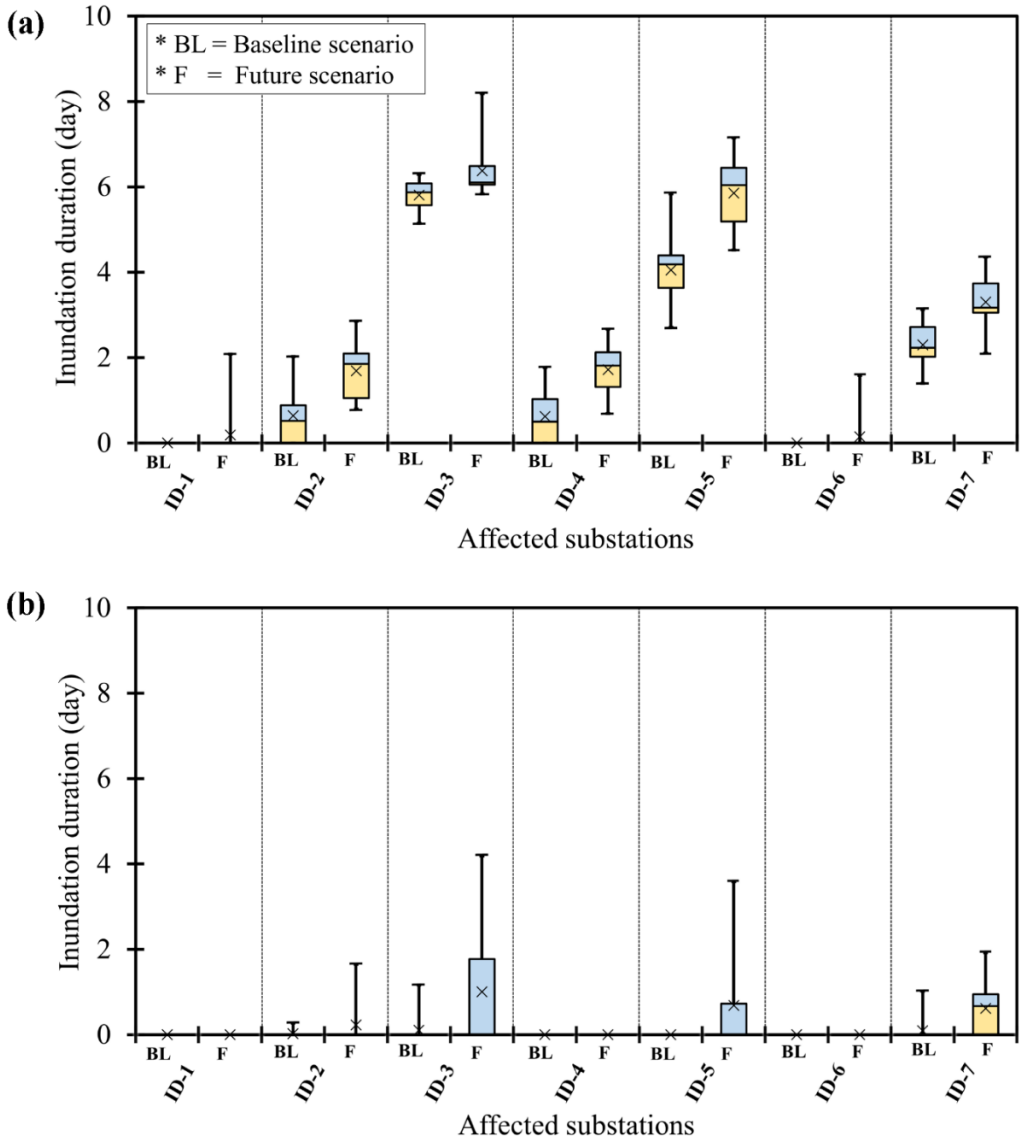

664

665 Figure 12. A summary of maximum inundation durations for substations that were
666 affected in the baseline and/or future periods (a) without flood protection measures and
667 (b) with flood protection measures. Note: Affected substations with their corresponding
668 IDs are shown in Figure 1. There are no negative values in the vertical axis, as the
669 minimum inundation duration is zero.

670

671 **4. Summary and Conclusion**

672 This paper applies an integrated modeling framework to evaluate climate change
673 impacts on flood regime, floodplain protection standards, and electricity infrastructures
674 across the Conasauga River Watershed in the southeastern United States. Building on the
675 ensemble concept used by Gangrade et al. (2019) for PMF-scale inundation modeling
676 (AEP < 10^{-4} %), we focused on more frequent extreme streamflow events (i.e., AEP
677 around 1–0.2%) based on 11 downscaled CMIP5 GCMs in this study. Our evaluation is
678 based on a climate-hydrologic-hydraulic modeling framework, which makes use of an
679 eleven member ensemble of downscaled climate simulations. Nine out of eleven
680 ensemble members project an increase in the flood inundation area in the future period.
681 Similarly, at the 1% AEP level, the flood inundation frequency curves indicate ~16 km^2
682 increase in floodplain area under the future climate. The comparison between the flood
683 depth frequency maps from the baseline and future simulations indicated that, on average,
684 ~80% of grid cells exhibit a 0.2 to 1.5 m increase in the flood depth values. Without the
685 flood protection measures, of the 44 electric substations inside the watershed, 5 and 7
686 substations could be affected during the baseline and future periods, respectively. Even
687 after flood-proofing, three and four substations could still be affected in the baseline and
688 future periods. The increases in flood depth magnitude and inundation duration at the
689 affected substations in the future period will most likely damage more electrical
690 components, inflate the cost of hardening measures and render substations out of service
691 for a longer period of time.

692 Although future climate conditions are uncertain, our results demonstrate the needs
693 for (1) consideration of climate change in the floodplain management regulations; (2)

694 improvements in the conventional deterministic flood delineation approach through the
695 inclusion of probabilistic or ensemble-based methods, and (3) improvements in the
696 existing flood protection measures for critical electricity infrastructures through enhanced
697 hydro-meteorologic modeling capacities. In particular, rapidly advanced high-
698 performance computing capabilities have enabled the incorporation of computationally
699 intensive 2D hydraulics modeling in the ensemble-based hydroclimate impact
700 assessment. While the computational cost demonstrated in this study may still seem
701 steep, in the current speed of technology advancement, we will soon be able to implement
702 such a computationally intensive assessment for wide applications. The approach
703 presented in this study can be used by floodplain managers to develop flood depth
704 frequency maps and to identify the most vulnerable electric substations.

705 **Author Contribution**

706 *Dullo*, *Kalyanapu*, *Kao*, *Gangrade* and *Morales-Hernández* developed the concept for the
707 paper, designed the methodology and *Dullo* performed all the simulations required for the
708 study with feedback from all the co-authors. *Sharif*, *Ghafoor* and *Morales-Hernández*
709 focused on programming, software development and testing of existing code components.
710 *Ashfaq* and *Morales-Hernández* provided access to supercomputing machine hours on
711 ORNL's SUMMIT and RHEA computers. The manuscript was edited by *Dullo* with inputs
712 from the co-authors.

713 **Competing Interests**

714 The authors declare that they have no conflict of interest.

715 **Acknowledgments**

This study was supported by the US Air Force Numerical Weather Modeling Program. TTD, MBS, AJK, and SG also acknowledge support by the Center of Management, Utilization, and Protection of Water Resources at Tennessee Technological University. Some portion of the project was funded by the UT Battelle Subcontract No: 4000164401. The research used resources of the Oak Ridge Leadership Computing Facility at Oak Ridge National Laboratory. Some of the co-authors are employees of UT-Battelle LLC under contract DE-AC05-00OR22725 with the US Department of Energy. Accordingly, the US government retains and the publisher, by accepting the article for publication, acknowledges that the US government retains a nonexclusive, paid-up, irrevocable, worldwide license to publish or reproduce the published form of this manuscript, or allow others to do so, for US government purposes. The input data sets are cited throughout the paper, as appropriate.

Data Availability

The data that support the findings of this study are openly available in figshare repository at the following URL: https://figshare.com/projects/Conasauga_Flood_Modeling_Project/80840.

References

AECOM: The Impact of Climate Change and Population Growth on the National Flood Insurance Program through 2100, available at: https://www.aecom.com/content/wp-content/uploads/2016/06/ Climate_Change_Report_AECOM_2013-06-11.pdf (last access: 12 October 2019), 2013.

737 Alfieri, L., Salamon, P., Bianchi, A., Neal, J., Bates, P., and Feyen, L.: Advances in Pan-
738 European Flood Hazard Mapping, Hydrol. Process., 28(13), 4067–4077,
739 doi:10.1002/hyp.9947, 2014.
740 Alfieri, L., Burek, P., Feyen, L., and Forzieri, G.: Global Warming Increases the
741 Frequency of River Floods in Europe, Hydrol. Earth Syst. Sci., 19, 2247–2260,
742 doi:10.5194/hess-19-2247-2015, 2015a.
743 Alfieri, L., Feyen, L., Dottori, F., and Bianchi, A.: Ensemble Flood Risk Assessment in
744 Europe Under High End Climate Scenarios, Global Environ. Chang., 35, 199–212,
745 doi:10.1016/j.gloenvcha.2015.09.004, 2015b.
746 Alfieri, L., Bisselink, B., Dottori, F., Naumann, G., de Roo, A., Salamon, P., Wyser, K.,
747 and Feyen, L.: Global Projections of River Flood Risk in a Warmer World, Earth's
748 Future, 5, 171–182, doi:10.1002/2016EF000485, 2017.
749 Alfieri, L., Dottori, F., Betts, R., Salamon, P., and Feyen, L.: Multi-Model Projections of
750 River Flood Risk in Europe under Global Warming, Climate, 6(6),
751 doi:10.3390/cli6010006, 2018.
752 Allen-Dumas, M. R., Binita, K. C., and Cunliff, C. I.: Extreme Weather and Climate
753 Vulnerabilities of the Electric Grid: A Summary of Environmental Sensitivity
754 Quantification Methods, ORNL/TM-2019/1252, Oak Ridge National Laboratory,
755 available at: https://www.energy.gov/sites/prod/files/2019/09/f67/
756 Oak%20Ridge%20National%20Laboratory%20EIS%20Response.pdf (last access: 17
757 December 2019), 2019.

758 Anderson, T. W., and Darling, D. A. Asymptotic theory of certain 'goodness-of-fit'
759 criteria based on stochastic processes, Ann. Math, Stat., 23, 193-212, 1952. URL:
760 https://www.jstor.org/stable/2236446
761 Archuleta, C.-A. M., Constance, E. W., Arundel, S. T., Lowe, A. J., Mantey, K. S., and
762 Phillips, L. A.: The National Map Seamless Digital Elevation Model Specifications,
763 US Geological Survey Techniques and Methods 11-B9, doi:10.3133/tm11B9,
764 available at: https://pubs.er.usgs.gov/publication/tm11B9 (last access: 31 December
765 2019), 2017.
766 Arnell, N. W. and Gosling, S. N.: The Impacts of Climate Change on River Flood Risk at
767 the Global Scale, Clim. Change, 134, 387–401, doi.10.1007/s10584-014-1084-5,
768 2014.
769 Ashfaq, M., Bowling, L. C., Cherkauer, K., Pal, J. S., and Diffenbaugh, N. S.: Influence
770 of Climate Model Biases and Daily-scale Temperature and Precipitation Events on
771 Hydrological Impacts Assessment: A Case Study of the United States, J. Geophys.
772 Res., 115, D14116, doi:10.1029/2009JD012965, 2010.
773 Ashfaq, M., Ghosh, S., Kao, S.-C., Bowling, L. C., Mote, P., Touma, D., Rauscher, S. A.,
774 and Diffenbaugh, N. S.: Near-term Acceleration of Hydroclimatic Change in the
775 Western U.S., J. Geophys. Res., 118, 10,676–10, 693, doi:10.1002/jgrd.50816, 2013.
776 Ashfaq, M., Rastogi, D., Mei, R., Kao, S.-C., Gangrade, S., Naz, B. S., and Touma, D.:
777 High-resolution Ensemble Projections of Near-term Regional Climate over the
778 Continental United States. J. Geophys. Res., 121, 9943–9963,
779 doi:10.1002/2016JD025285, 2016.

780 Baechler, M. C., Gilbride, T. L., Cole, P. C., Hefty, M. G., and Ruiz, K.: Building
781 America Best Practices Series, Volume 7.3, High-Performance Home Technologies:
782 Guide to Determining Climate Regions by County, Pacific Northwest National
783 Laboratory, US Department of Energy under Contract DE-AC05-76RLO 1830,
784 PNNL-17211 Rev. 3, available at:
785 https://www.energy.gov/sites/prod/files/2015/10/f27/ba_climate_region_guide_7.3.pd
786 f (last access: 27 September 2020), 2015.
787 Bhuyian, Md. N. M., Kalyanapu, A. J., and Nardi, F.: Approach to Digital Elevation
788 Model Correction by Improving Channel Conveyance, J. Hydrol. Eng., 20(5),
789 doi:10.1061/(ASCE)HE.1943-5584.0001020, 2014.
790 Bhuyian, Md. N. M., Dullo, T. T., Kalyanapu, A. J., Gangrade, S., and Kao, S.–C.:
791 Application of Geomorphic Correlations for River Bathymetry Correction in Two-
792 dimensional Hydrodynamic Modeling for Long-term Flood Risk Evaluation, World
793 Environmental and Water Resources Congress, Pittsburgh, Pennsylvania, USA, 19-23
794 May 2019, 2019.
795 Birhanu, D., Kim, H., Jang, C., and Park, S.: Flood Risk and Vulnerability of Addis
796 Ababa City Due to Climate Change and Urbanization, Procedia Engineer., 154, 696–
797 702, doi:10.1016/j.proeng.2016.07.571, 2016.
798 Blessing, R., Sebastian, A., and Brody, S. D.: Flood Risk Delineation in the United
799 States: How Much Loss Are We Capturing?, Nat. Hazards Rev., 18(3), 04017002-(1-
800 10), doi:10.1061/(ASCE)NH.1527-6996.0000242, 2017.

Bollinger, L. A. and Dijkema, G. P. J.: Evaluating Infrastructure Resilience to Extreme Weather – the Case of the Dutch Electricity Transmission Network, EJTIR, 16(1), 214–239, doi:10.18757/ejtir.2016.16.1.3122, 2016.

Bragatto, T., Cresta, M., Cortesi, F., Gatta, F. M., Geri, A., Maccioni, M., and Paulucci, M.: Assessment and Possible Solution to Increase Resilience: Flooding Threats in Terni Distribution Grid, Energies, 12(4), 744, doi:10.3390/en12040744, 2019.

Brunner, G. W., Warner, J. C., Wolfe, B. C., Piper, S. S., and Marston, L.: Hydrologic Engineering Center – River Analysis System (HEC-RAS) Applications Guide 2016, Version 5.0, US Army Corps of Engineers, CA, available at: https://www.hec.usace.army.mil/software/hec-ras/documentation/HEC-RAS%205.0%20Applications%20Guide.pdf (last access: 27 December 2019), 2016.

Burkey, J.: Log-Pearson Flood Flow Frequency using USGS 17B, available at: https://www.mathworks.com/matlabcentral/fileexchange/22628-log-pearson-flood-flow-frequency-using-usgs-17b (last access: 23 December 2019), 2009.

Chandramowli, S. N. and Felder, F. A.: Impact of Climate Change on Electricity Systems and Markets – A Review of Models and Forecasts, Sustain. Energy Technol. Assess., 5, 62–74, doi:10.1016/j.seta.2013.11.003, 2014.

Ciscar, J. C. and Dowling, P.: Integrated Assessment of Climate Impacts and Adaptation in the Energy Sector, Energy Econ., 46, 531–538, doi:10.1016/j.eneco.2014.07.003, 2014.

Cronin, J., Anandarajah, G., and Dessens, O.: Climate Change Impacts on the Energy System: A Review of Trends and Gaps, Clim. Change, 151, 79–93, doi:10.1007/s10584-018-2265-4, 2018.

824 Cook, A. and Merwade, V.: Effect of topographic data, geometric configuration and
825 modeling approach on flood inundation mapping, J. Hydrol., 377(1-2), 131-142,
826 doi:10.1016/j.jhydrol.2009.08.015, 2009.
827 Daly, C., Halbleib, M., Smith, J. I., Gibson, W. P., Doggett, M. K., Taylor, G. H., Curtis,
828 J., and Pasteris, P. P.: Physiographically Sensitive Mapping of Climatological
829 Temperature and Precipitation Across the Conterminous United States, Int. J.
830 Climatol., 28(15), 2031–2064, doi:10.1002/joc.1688, 2008.
831 Dey, S., Saksena, S., and Merwade, V.: Assessing the effect of different bathymetric
832 models on hydraulic simulation of rivers in data sparse regions, J. Hydrol., 575, 838-
833 851, doi:10.1016/j.jhydrol.2019.05.085, 2019.
834 Elliott, K. J. and Vose, J. M.: Initial Effects of Prescribed Fire on Quality of Soil Solution
835 and Streamwater in the Southern Appalachian Mountains, South. J. Appl. For., 29(1),
836 5–15, doi:10.1093/sjaf/29.1.5, 2005.
837 Elsner, M. M., Cuo, L., Voisin, N., Deems, J. S., Hamlet, A. F., Vano, J. A., Mickelson,
838 K. E. B., Lee, S.-Y., and Lettenmaier, D. P.: Implications of 21st Century Climate
839 Change for the Hydrology of Washington State, Climatic Change, 102(1–2), 225–
840 260, doi:10.1007/s10584-010-9855-0, 2010.
841 EMA (Emergency Management Agency): Whitfield County Hazard Mitigation Plan
842 2016, Including the Cities of Dalton, Tunnel Hill, and Varnell, and the Town of
843 Cohutta, Whitfield County Emergency Management Agency, available at:
844 https://www.whitfieldcountyga.com/ema/WhitfieldHMPDraft52616.pdf (last access:
845 29 March 2020), 2016.

England Jr., J. F., Cohn, T. A., Faber, B. A., Stedinger, J. R., Thomas Jr., W. O., Veilleux, A. G., Kiang, J. E., and Mason Jr., R. R.: Guidelines for Determining Flood Flow Frequency—Bulletin 17C, Techniques and Methods 4-B5, US Geological Survey, https://doi.org/10.3133/tm4B5, 2019.

Farber-DeAnda, M., Cleaver, M., Lewandowski, C., and Young, K.: Hardening and Resiliency: US Energy Industry Response to Recent Hurricanes Seasons, Office of Electricity Delivery and Energy Reliability, US Department of Energy, available at: https://www.oe.netl.doe.gov/docs/HR-Report-final-081710.pdf (last access: 17 December 2019), 2010.

FEMA (Federal Emergency Management Agency): National Flood Insurance Program: Program Description, Federal Emergency Management Agency, available at: https://www.fema.gov/media-library-data/20130726-1447-20490-2156/nfipdescrip_1_.pdf (last access: 22 January 2018), 2002.

FEMA (Federal Emergency Management Agency): Emergency Power Systems for Critical Facilities: A Best Practices Approach to Improving Reliability, FEMA P-1019, Applied Technology Council, Redwood City, CA, available at: https://www.fema.gov/media-library/assets/documents/101996 (last access: 17 December 2019), 2014.

FEMA (Federal Emergency Management Agency): FEMA Flood Map Service Center, available at: https://msc.fema.gov/portal/ availabilitySearch?#searchresultsanchor (last access: 28 December 2019), 2019.

FIS (Flood Insurance Study): Flood Insurance Study: Whitfield County, Georgia and Incorporated Areas, Flood Insurance Study Number: 13313CV000A, Federal

Emergency Management Agency, available at: http://www.georgiadfirm.com/pdf/panels/13313CV000A.pdf (last access: 25 December 2019), 2007.

FIS (Flood Insurance Study): Flood Insurance Study: Murray County, Georgia and Incorporated Areas, Flood Insurance Study Number: 13213CV000A, Federal Emergency Management Agency, available at: http://www.georgiadfirm.com/pdf/panels/13213CV000A.pdf (last access: 27 December 2019), 2010.

Forzieri, G., Bianchi, A., e Silva, F. B., Herrera, M. A. M., Leblois, A., Lavalle, C., Aerts, J. C. J. H., and Feyen, L.: Escalating Impacts of Climate Extremes on Critical Infrastructures in Europe, Glob. Environ. Change, 48, 97–107, doi:10.1016/j.gloenvcha.2017.11.007, 2018.

Fu, G., Wilkinson, S., Dawson, R. J., Fowler, H. J., Kilsby, C., Panteli, M., and Mancarella, P.: Integrated Approach to Assess the Resilience of Future Electricity Infrastructure Networks to Climate Hazards, IEEE Syst. J., 12(4), 3169–3180, doi:10.1109/JSYST.2017.2700791, 2017.

Galloway, G. E., Baecher, G. B., Plasencia, D., Coulton, K. G., Louthain, J., Bagha, M., and Levy, A. R.: Assessing the Adequacy of the National Flood Insurance Program's 1 Percent Flood Standard, Water Policy Collaborative, University of Maryland, available at: https://www.fema.gov/media-library/assets/documents/9594 (last access: 17 December 2019), 2006.

Gangrade, S., Kao, S.-C., Naz, B. S., Rastogi, D., Ashfaq, M., Singh, N., and Preston, B. L.: Sensitivity of Probable Maximum Flood in a Changing Environment, Water Resour. Res., 54(6), 3913–3936, doi:10.1029/2017WR021987, 2018.

Gangrade, S., Kao, S.-C., Dullo, T. T., Kalyanapu, A. J., and Preston, B. L.: Ensemble-based Flood Vulnerability Assessment for Probable Maximum Flood in a Changing Environment, J. Hydrol., 576, 342–355, doi:10.1016/j.jhydrol.2019.06.027, 2019.

Gangrade, S., Kao, S.-C., and McManamay, R. A.: Multi-model Hydroclimate Projections for the Alabama-Coosa-Tallapoosa River Basin in the Southeastern United States, Sci. Rep., 10, 2870, doi:10.1038/s41598-020-59806-6, 2020.

Gilstrap, M., Amin, S., and DeCorla-Souza, K.: United States Electricity Industry Primer, DOE/OE-0017, Office of Electricity Delivery and Energy Reliability, US Department of Energy, Washington DC, available at: https://www.energy.gov/sites/prod/files/2015/12/f28/united-states-electricity-industry-primer.pdf (last access: 17 December 2019), 2015.

Giorgi, F., Coppola, E., Solmon, F., Mariotti, L., Sylla, M. B., Bi, X., Elguindi, N., Diro, G. T., Nair, V., Giuliani, G., Turuncoglu, U. U., Cozzini, S., Güttler, I., O'Brien, T. A., Tawfik, A. B., Shalaby, A., Zakey, A. S., Steiner, A. L., Stordal, F., Sloan, L. C., and Brankovic, C.: RegCM4: model description and preliminary tests over multiple CORDEX domains, Climate Res., 52, 7–29, doi:10.3354/cr01018, 2012.

HCFCD (Harris County Flood Control District): Hurricane Harvey – Storm and Flood Information, available at: https://www.hcfcd.org/Portals/62/Harvey/immediate-flood-report-final-hurricane-harvey-2017.pdf (last access: 16 December 2019), 2018.

HIFLD (Homeland Infrastructure Foundation-Level Data): Homeland Infrastructure Foundation-Level Data, Electric Substations, US Department of Homeland Security, available at: https://hifld-geoplatform.opendata.arcgis.com/ datasets/electric-substations (last access: 20 December 2019), 2019.

Hirabayashi, Y., Mahendran, R., Koirala, S., Konoshima, L., Yamazaki, D., Watanabe, S., Kim, H., and Kanae, S.: Global Flood Risk under Climate Change, Nature Clim. Chang., 3, 816–821, doi:10.1038/NCLIMATE1911, 2013.

Hou, Z., Ren, H., Sun, N., Wigmosta, M. S., Liu, Y., Leung, L. R., Yan, H., Skaggs, R., and Coleman, A.: Incorporating Climate Nonstationarity and Snowmelt Processes in Intensity–Duration–Frequency Analyses with Case Studies in Mountainous Areas, J. Hydrometeorol., 20(12), 2331–2346, doi:10.1175/JHM-D-19-0055.1, 2019.

Ivey, G. and Evans, K.: Conasauga River Alliance Business Plan: Conasauga River Watershed Ecosystem Project, available at: https://www.fs.fed.us/largewatershedprojects/businessplans/ (last access: 22 December 2019), 2000.

Kalyanapu, A. J., Burian, S. J., and McPherson, T. N.: Effect of Land Use-Based Surface Roughness on Hydrologic Model Output, Journal of Spatial Hydrology, 9(2), 51–71, 2009.

Kalyanapu, A. J., Shankar, S., Pardyjak, E. R., Judi, D. R., and Burian, S. J.: Assessment of GPU Computational Enhancement to a 2D Flood Model, Environ. Modell. Softw., 26(8), 1009–1016, doi:10.1016/j.envsoft.2011.02.014, 2011.

Kefi, M., Mishra, B. K., Kumar, P., Masago, Y., and Fukushi, K.: Assessment of Tangible Direct Flood Damage Using a Spatial Analysis Approach under the Effects

of Climate Change: Case Study in an Urban Watershed in Hanoi, Vietnam, Int. J. Geo-Inf., 7, 29, doi:10.3390/ijgi7010029, 2018.

Kollat, J. B., Kasprzyk, J. R., Thomas Jr., W. O., Miller, A. C., and Divoky, D.: Estimating the Impacts of Climate Change and Population Growth on Flood Discharges in the United States, J. Water Resour. Plann. Manage., 138(5), 442–452, doi:10.1061/(ASCE)WR.1943-5452.0000233, 2012.

Langerwisch, F., Rost, S., Gerten, D., Poulter, B., Rammig, A., and Cramer, W.: Potential Effects of Climate Change on Inundation Patterns in the Amazon Basin, Hydrol. Earth Syst. Sci., 17, 2247–2262, doi:10.5194/hess-17-2247-2013, 2013.

Li, H., Sun, J., Zhang, H., Zhang, J., Jung, K., Kim, J., Xuan, Y., Wang, X., and Li, F.: What Large Sample Size Is Sufficient for Hydrologic Frequency Analysis? – A Rational Argument for a 30-Year Hydrologic Sample Size in Water Resources Management, Water, 10, 430, doi:10.3390/w10040430, 2018.

Marshall, R., Ghafoor, S., Rogers, M., Kalyanapu, A., and Dullo, T. T.: Performance Evaluation and Enhancements of a Flood Simulator Application for Heterogeneous HPC Environments, Int. J. Network Comput., 8(2), 387–407, 2018.

McCuen, R. H.: Hydrologic Analysis and Design, Third Edition, Pearson-Prentice Hall, Upper Saddle River, New Jersey, 2005.

Mikellidou, C. V., Shakou, L. M., Boustras, G., and Dimopoulos, C.: Energy Critical Infrastructures at Risk from Climate Change: A State of the Art Review, Saf. Sci., 110, 110–120, doi:10.1016/j.ssci.2017.12.022, 2018.

Milly, P. C. D., Wetherald, R. T., Dunne, K. A., and Delworth, T. L.: Increasing Risk of Great Floods in a Changing Climate, Nature, 415(6871), 514–517, doi:10.1038/415514a, 2002.

Mora, C., Spirandelli, D., Franklin, E. C., Lynham, J., Kantar, M. B., Miles, W., Smith, C. Z., Freel, K., Moy, J., Louis, L. V., Barba, E. W., Bettinger, K., Frazier, A. G., Colburn IX, J. F., Hanasaki, N., Hawkins, E., Hirabayashi, Y., Knorr, W., Little, C. M., Emanuel, K., Sheffield, J., Patz, J. A., and Hunter, C. L.: Broad Threat to Humanity from Cumulative Climate Hazards Intensified by Greenhouse Gas Emissions, Nature Clim. Chang., 8, 1062–1071, doi:10.1038/s41558-018-0315-6, 2018.

Morales-Hernández, M., Sharif, M. B., Gangrade, S., Dullo, T. T., Kao, S.-C., Kalyanapu, A., Ghafoor, S. K., Evans, K. J., Madadi-Kandjani, E., and Hodges, B. R.: High Performance Computing in Water Resources Hydrodynamics, Journal of Hydroinformatics, in press, 2020.

Morales-Hernández, M., Sharif, Md. B., Kalyanapu, A., Ghafoor, S. K., Dullo, T.T., Gangrade, S., Kao, S.-C., Norman, M. R., and Evans, K. J.: TRITON: A Multi-GPU Open Source 2D Hydrodynamic Flood, Environmental Modelling & Software, in press, 2021.

MRLC (Multi-Resolution Land Characteristics Consortium): National Land Cover Database (NLCD), available at: https://www.mrlc.gov/data/nlcd-2011-land-cover-conus-0 (last access: 5 May 2020), 2011.

NERC (North American Electric Reliability Corporation): Hurricane Harvey Event Analysis Report, North American Electric Reliability Corporation, Atlanta, GA,

available at: https://www.nerc.com/pa/rrm/ea/Hurricane_Harvey_EAR_DL/NERC_Hurricane_Harvey_EAR_20180309.pdf (last access: 17 December 2019), 2018.

Ntelekos, A. A., Oppenheimer, M., Smith, J. A., and Miller, A. J.: Urbanization, Climate Change and Flood Policy in the United States, Clim. Chang., 103, 597–616, doi:10.1007/s10584-009-9789-6, 2010.

Nyaupane, N., Thakur, B., Kalra, A., and Ahmad, S.: Evaluating Future Flood Scenarios Using CMIP5 Climate Projections, Water, 10, 1866, doi:10.3390/w10121866, 2018.

Olsen, J. R.: Climate Change and Floodplain Management in the United States, Clim. Change, 76, 407–426, doi:10.1007/s10584-005-9020-3, 2006.

Pachauri, R. K. and Meyer, L. A.: Intergovernmental Panel on Climate Change (IPCC): Climate Change 2014: Synthesis Report, in Proceedings of Contribution of Working Groups I, II and III to the Fifth Assessment Report of the Intergovernmental Panel on Climate Change, Geneva, Switzerland, available at: https://www.ipcc.ch/site/assets/uploads/2018/05/SYR_AR5_FINAL_full_wcover.pdf (last access: 16 December 2019), 2014.

Pant, R., Thacker, S., Hall, J. W., Alderson, D., and Barr, S.: Critical Infrastructure Impact Assessment Due to Flood Exposure, J. Flood Risk Manag., 11, 22–33, doi:10.1111/jfr3.12288, 2017.

Pielke Jr., R. A. and Downton, M. W.: Precipitation and Damaging Floods: Trends in the United States, 1932–97, J. Climate, 13(20), 3625–3637, doi:10.1175/1520-0442(2000)013<3625:PADFTI>2.0.CO;2, 2000.

1000 Pielke Jr., R. A., Downton, M. W., and Barnard Miller, J. Z.: Flood Damage in the United
1001 States, 1926-2000: A reanalysis of National Weather Service Estimates, National
1002 Center for Atmospheric Research, Boulder, CO, available at:
1003 https://sciencepolicy.colorado.edu/flooddamagedata/flooddamagedata.pdf (last
1004 access: 16 December 2019), 2002.
1005 Pralle, S.: Drawing Lines: FEMA and the Politics of Mapping Flood Zones, Clim.
1006 Chang., 152, 227–237, doi:10.1007/s10584-018-2287-y, 2019.
1007 Reed, D. A., Kapur, K. C., and Christie, R. D.: Methodology for Assessing the Resilience
1008 of Networked Infrastructure, IEEE Syst. J., 3(2), 174–180,
1009 doi:10.1109/JSYST.2009.2017396, 2009.
1010 Saksena, S., Dey, S., Merwade, V., & Singhofen, P. J. (2020). A computationally
1011 efficient and physically based approach for urban flood modeling using a flexible
1012 spatiotemporal structure. Water Resources Research, 56, e2019WR025769.
1013 https://doi.org/10.1029/2019WR025769
1014 Storck, P., Bowling, L., Wetherbee, P., and Lettenmaier, D.: Application of a GIS-Based
1015 Distributed Hydrology Model for Prediction of Forest Harvest Effects on Peak
1016 Stream Flow in the Pacific Northwest, Hydrol. Process., 12(6), 889–904,
1017 doi:10.1002/(SICI)1099-1085(199805)12:6<889::AID-HYP661>3.0.CO;2-P, 1998.
1018 Strauss, B. and Ziemlinski, R.: Sea Level Rise Threats to Energy Infrastructure: A
1019 Surging Seas Brief Report by Climate Central, Climate Central, Washington, DC,
1020 available at: http://slr.s3.amazonaws.com/SLR-Threats-to-Energy-Infrastructure.pdf
1021 (last access: 17 December 2019), 2012.

Tan, A.: Sandy and Its Impacts: Chapter 1, NYC Special Initiative for Rebuilding and Resiliency, NYC Resources, NY, available at: http://www.nyc.gov/html/sirr/downloads/pdf/final_report/Ch_1_SandyImpacts_FINAL_singles.pdf (last access: 17 December 2019), 2013.

Thornton, P. E., Running, S. W., and White, M. A.: Generating surfaces of daily meteorological variables over large regions of complex terrain, J. Hydrol., 190, 214–251, doi:10.1016/S0022-1694(96)03128-9, 1997.

UNISDR (United Nations Office for Disaster Risk Reduction): Making Development Sustainable: The Future of Disaster Risk Management, Global Assessment Report on Disaster Risk Reduction, Geneva, Switzerland, available at: https://www.preventionweb.net/english/hyogo/gar/2015/en/gar-pdf/GAR2015_EN.pdf (last access: 16 December 2019), 2015.

USACE (US Army Corps of Engineers): Master Water Control Manual: Alabama-Coosa-Tallapoosa (ACT) River Basin, Alabama, Georgia, US Army Corps of Engineers, available at: https://www.sam.usace.army.mil/Portals/46/docs/planning_environmental/act/docs/New/ACT%20Master%20Manual_March%2013.pdf (last access: 22 December 2019), 2013.

USGS (US Geological Survey): Guidelines for Determining Flood Flow Frequency, Bulletin #17B of the Hydrology Subcommittee, Interagency Advisory Committee on Water Data, US Geological Survey, Reston, VA, 1982.

Vale, M.: Securing the US Electrical Grid, Center for the Study of the Presidency and Congress (CSPC), Washington DC, available at: https://protectourpower.org/resources/cspc-2014.pdf (last access: 14 March 2017), 2014.

Wigmosta, M. S., Vail, L. W., and Lettenmaier, D. P.: A Distributed Hydrology-Vegetation Model for Complex Terrain, Water Resour. Res., 30(6), 1665–1679, doi:10.1029/94WR00436, 1994.

Wigmosta, M. S., Nijssen, B., Storck, P., and Lettenmaier, D. P.: The Distributed Hydrology Soil Vegetation Model, in Mathematical Models of Small Watershed Hydrology and Applications, V. P. Singh, D. K. Frevert, eds., Wat. Resour. Publications, Littleton, CO, 2002.

Wilbanks, T. J., Bhatt, V., Bilello, D., Bull, S., Ekmann, J., Horak, W., Huang, Y. J., Levine, M. D., Sale, M. J., Schmalzer, D., and Scott, M. J.: Effects of Climate Change on Energy Production and Use in the United States, US Climate Change Science Program Synthesis and Assessment Product 4.5, available at: https://digitalcommons.unl.edu/cgi/viewcontent.cgi?article=1005&context=usdoepub (last access: 17 December 2019), 2008.

Wing, O. E. J., Bates, P. D., Sampson, C. C., Smith, A. M., Johnson, K. A., and Erickson, T. A.: Validation of a 30 m Resolution Flood Hazard Model of the Conterminous United States, Water Resour. Res., 53, 7968–7986, doi:10.1002/2017WR020917, 2017.

Wing, O. E. J., Bates, P. D., Smith, A. M., Sampson, C. C., Johnson, K. A., Fargione, J., and Morefield, P.: Estimates of Present and Future Flood Risk in the Conterminous United States, Environ. Res. Lett., 13(3), 034023, doi:10.1088/1748-9326/aaac65, 2018.

Winkler, J., Duenas-Osorio, L., Stein, R., and Subramanian, D.: Performance Assessment of Topologically Diverse Power Systems Subjected to Hurricane Events, Reliability

Engineering and System Safety, 95(4), 323–336, doi:10.1016/j.ress.2009.11.002, 2010.

Winsemius, H. C., Aerts, J. C. J. H., van Beek, L. P. H., Bierkens, M. F. P., Bouwman, A., Jongman, B., Kwadijk, J. C. J., Ligtvoet, W., Lucas, P. L., van Vuuren, D. P., and Ward, P. J.: Global Drivers of Future River Flood Risk, Nat. Clim. Chang., 6, 381–385, doi:10.1038/NCLIMATE2893, 2016.

Wobus, C., Gutmann, E., Jones, R., Rissing, M., Mizukami, N., Lorie, M., Mahoney, H., Wood, A. W., Mills, D., and Martinich, J.: Climate Change Impacts on Flood Risk and Asset Damages within Mapped 100-year Floodplains of the Contiguous United States, Nat. Hazards Earth Syst. Sci., 17, 2199–2211, doi:10.5194/nhess-17-2199-2017, 2017.

Zamuda, C., Antes, M., Gillespie, C. W., Mosby, A., and Zotter, B.: Climate Change and the US Energy Sector: Regional Vulnerabilities and Resilience Solutions, Office of Energy Policy and Systems Analysis, US Department of Energy, available at: https://energy.gov/sites/prod/files/2015/10/f27/Regional_Climate_Vulnerabilities_and_Resilience_Solutions_0.pdf (last access: 17 December 2019), 2015.

Zamuda, C. and Lippert, A.: Climate Change and the Electricity Sector: Guide for Assessing Vulnerabilities and Developing Resilience Solutions to Sea Level Rise, Office of Energy Policy and Systems Analysis, US Department of Energy, available at: https://toolkit.climate.gov/sites/default/files/Climate%20Change%20and%20the%20Electricity%20Sector%20Guide%20for%20Assessing%20Vulnerabilities%20and%20Developing%20Resilience%20Solutions%20to%20Sea%20Level%20Rise%20July%202016.pdf (last access: 18 December 2019), 2016.

Zhao, G., Gao, H., Naz, B. S., Kao, S.-C., and Voisin, N.: Integrating a Reservoir Regulation Scheme into a Spatially Distributed Hydrological Model, Adv. Water Resour., 98, 16–31, doi:10.1016/j.advwatres.2016.10.014, 2016.

Zheng, X., Maidment, D. R., Tarboton, D. G., Liu, Y. Y., and Passalacqua, P.: GeoFlood: Large-scale Flood Inundation Mapping Based on High-Resolution Terrain Analysis, Water Resour. Res., 54, 10,013–10,033, doi:10.1029/2018WR023457, 2018.